National Library of Canada

Acquisitions and Bibliographic Services Branch

395 Wellington Street
Ottawa, Ontario
K1A 0N4

Bibliothèque nationale du Canada

Direction des acquisitions et des services bibliographiques

395, rue Wellington
Ottawa (Ontario)
K1A 0N4

*Your file Votre référence*

*Our file Notre référence*

**NOTICE**

**The quality of this microform is heavily dependent upon the quality of the original thesis submitted for microfilming. Every effort has been made to ensure the highest quality of reproduction possible.**

**If pages are missing, contact the university which granted the degree.**

**Some pages may have indistinct print especially if the original pages were typed with a poor typewriter ribbon or if the university sent us an inferior photocopy.**

**Reproduction in full or in part of this microform is governed by the Canadian Copyright Act, R.S.C. 1970, c. C-30, and subsequent amendments.**

**AVIS**

**La qualité de cette microforme dépend grandement de la qualité de la thèse soumise au microfilmage. Nous avons tout fait pour assurer une qualité supérieure de reproduction.**

**S'il manque des pages, veuillez communiquer avec l'université qui a conféré le grade.**

**La qualité d'impression de certaines pages peut laisser à désirer, surtout si les pages originales ont été dactylographiées à l'aide d'un ruban usé ou si l'université nous a fait parvenir une photocopie de qualité inférieure.**

**La reproduction, même partielle, de cette microforme est soumise à la Loi canadienne sur le droit d'auteur, SRC 1970, c. C-30, et ses amendements subséquents.**

Canada

UNIVERSITY OF ALBERTA

# MICROMACHINED CENTER TAPS FOR SILICON V-GROOVE WAVEGUIDES

BY

MING-YEE (EMMA) FEI

©

A thesis submitted to the Faculty of Graduate Studies and Research in partial fulfillment of the requirements for the degree of **MASTER OF SCIENCE**.

DEPARTMENT OF ELECTRICAL ENGINEERING

EDMONTON, ALBERTA

SPRING 1993

National Library
of Canada

Acquisitions and
Bibliographic Services Branch

395 Wellington Street
Ottawa, Ontario
K1A 0N4

Bibliothèque nationale
du Canada

Direction des acquisitions et
des services bibliographiques

395, rue Wellington
Ottawa (Ontario)
K1A 0N4

*Your file Votre référence*

*Our file Notre référence*

**The author has granted an irrevocable non-exclusive licence allowing the National Library of Canada to reproduce, loan, distribute or sell copies of his/her thesis by any means and in any form or format, making this thesis available to interested persons.**

**L'auteur a accordé une licence irrévocable et non exclusive permettant à la Bibliothèque nationale du Canada de reproduire, prêter, distribuer ou vendre des copies de sa thèse de quelque manière et sous quelque forme que ce soit pour mettre des exemplaires de cette thèse à la disposition des personnes intéressées.**

**The author retains ownership of the copyright in his/her thesis. Neither the thesis nor substantial extracts from it may be printed or otherwise reproduced without his/her permission.**

**L'auteur conserve la propriété du droit d'auteur qui protège sa thèse. Ni la thèse ni des extraits substantiels de celle-ci ne doivent être imprimés ou autrement reproduits sans son autorisation.**

ISBN 0-315-82206-6

Canada

UNIVERSITY OF ALBERTA

RELEASE FORM

NAME OF AUTHOR: **MING-YEE (EMMA) FEI**

TITLE OF THESIS: **MICROMACHINED CENTER TAPS FOR SILICON V-GROOVE WAVEGUIDES**

DEGREE: **MASTER OF SCIENCE**

YEAR THIS DEGREE GRANTED: **1993**

Permission is hereby granted to the University of Alberta Library to reproduce single copies of this thesis and to lend or sell such copies for private, scholarly or scientific research purposes only.

The author reserves all other publication and other rights in association with the copyright in the thesis, and except as hereinbefore provided neither the thesis nor any substantial portion thereof may be printed or otherwise reproduced in any material form whatever without the author's prior written permission.

Ming-Yee (Emma) Fei
11248 - 10 Avenue
Edmonton, Alberta
Canada T6J 6S2

Date: Mar 16, 1993

UNIVERSITY OF ALBERTA

FACULTY OF GRADUATE STUDIES AND RESEARCH

The undersigned certify that they have read, and recommend to the Faculty of Graduate Studies and Research for acceptance, a thesis entitled **MICROMACHINED CENTER TAPS FOR SILICON V-GROOVE WAVEGUIDES** submitted by **MING-YEE (EMMA) FEI** in partial fulfillment of the requirements for the degree of **MASTER OF SCIENCE**.

Dr. R. I. MacDonald, Supervisor

Dr. J. N. McMullin, Supervisor

Dr. R. Fedosejevs, Examiner

Dr. W. Allegretto, External Examiner

Date: Mar. 11, 1993.

## ABSTRACT

A new method has been developed for the fabrication of integrated out-of-plane taps in silicon v-groove waveguide. Experiments were conducted which determined the etching mechanism and the important etching rates were measured. A method for designing center taps with specific tapping ratios is proposed. Out-of-plane tapping has been demonstrated and the optical properties of the tapped waveguides have been analyzed.

## Acknowledgements

I would like to express my gratitude to my supervisors Dr. J. N. McMullin and Dr. R. I. MacDonald, for their support and guidance throughout this project. I have benefited greatly from their advice and encouragement.

I thank the Telecommunication Research Laboratories (TRLabs) for the scholarship and the measurement facility. I owe the successful completion of this project to Alberta Microelectronic Center (AMC), for their support and process facility. I thank the Department of Electrical Engineering of the University of Alberta for the Teaching Assistantship and other facilities.

I would like to thank Graham McKinnon for arranging for all necessary resources at the AMC to complete this project. I also thank him for the help and advice given at the various stages of this project.

I would also like to thank the following people for their assistance:
Glen Fitzpatrick, AMC, for his co-operation and immense help with the CVD processing, assistance in the development of a process for the "home-made" alignment marks, and for the SEM picture.
Yan Loke, AMC, for his co-operation and immense help with the photolithography process, silicon micromachining and for the constant help and encouragement.
Alan Mitchell, AMC, for electron beam evaporation of aluminum.
Dr. Barry Keyworth, TRLabs, for his immense help with the measurement set-up.
Senthil Kumar, my colleague, for the help and useful discussion.
Rajashree Narendra, my colleague, for helpful discussion.
Michael Konevecki for his help in RIE processing and helpful discussion.
Makarand Paranjape for his help and proof reading.

Finally, I thank my family and friends for all the co-operation and help they have extended.

# Table of Contents


Chapter 1. Introduction ..... 1
1.1. History and applications of optoelectronic integrated circuits ..... 1
1.2. Waveguides in OEICs ..... 4
1.3. An integrated out-of-plane tap ..... 5
1.4. Outline of Thesis ..... 9
Chapter 2. Design of Integrated Center Taps ..... 10
2.1. The development of a center tap ..... 10
2.2. Determination of etch rate for center taps ..... 14
2.3. Design of a tap with a specified tapping ratio ..... 28
2.4. Design of taps in a waveguide with various tapping ratios ..... 32
Chapter 3. Tap Fabrication ..... 35
3.1. Discovery of fabrication method, masking pattern and material ..... 35
3.2. Photolithography ..... 43
3.3. Anisotropic etching ..... 43
3.4. Deposition of the lower cladding layer ..... 44
3.5. Metallization of coupling planes ..... 45
3.6. Application of core material ..... 45
3.7. Application of cladding ..... 46
3.8. End polishing for butt-coupling ..... 46
Chapter 4. Optical Properties of Waveguides with Center Taps ..... 48
4.1. Introduction to the measurement method ..... 48
4.2. Measurement setup ..... 49
4.3. Waveguide tap measurement results ..... 52
4.4. Analysis of the measured data ..... 58
4.5. Comparison of the analyzed data ..... 66
Chapter 5. Conclusions ..... 70
5.1. Summary of work ..... 70
5.2. Suggestions for future work ..... 71
Bibliography ..... 73
APPENDIX A THE PROCEDURE OF HOME MADE ALIGNMENT MARKS ..... 75
APPENDIX B CALCULATION FOR THEORETICAL TAPPING RATIO AND CORRECTION FACTOR FOR POLYMER DEPRESSION ..... 76

# List of Tables


| | | |
|---|---|---|
| Table 4.1 | Scattering loss measurement results from both fiber probe and photodetector | 59 |
| Table 4.2 | Theoretical tapping ratios and analyzed results from Method A and B | 62 |
| Table 4.3 | Analyzed data obtained from Method C | 63 |

## List of Figures


| | | |
|---|---|---|
| Figure 1.1 | The schematic of OEIC switch matrix with optical waveguides and out-of-plane taps | 3 |
| Figure 1.2 | A v-groove waveguide with end facet tapping | 6 |
| Figure 1.3a | Mask pattern for a v-groove waveguide with a sidewall tap and an end facet | 8 |
| Figure 1.3b | V-groove and sidewall tap and an end facet after EDP etching | 8 |
| Figure 2.1a | The basic concept of a center tap in a waveguide (Top View) | 11 |
| Figure 2.1b | The basic concept of a center tap in a waveguide (Side View) | 11 |
| Figure 2.2 | The concept of a center tap formation by undercutting | 13 |
| Figure 2.3a | Observation of a center tap formation in EDP etching (Side View) | 13 |
| Figure 2.3b | End view of a center tap in a v-groove waveguide | 13 |
| Figure 2.4a | SEM photograph of a center tap with initial barrier of 39 μm etched for 4 minutes | 16 |
| Figure 2.4b | SEM photograph of a center tap with initial barrier of 39 μm etched for 8 minutes | 16 |
| Figure 2.4c | SEM photograph of a center tap with initial barrier of 39 μm etched for 12 minutes | 17 |
| Figure 2.4d | SEM photograph of a center tap with initial barrier of 39 μm etched for 16 minutes | 17 |
| Figure 2.4e | SEM photograph of a center tap with initial barrier of 5 μm etched for 8 minutes | 18 |
| Figure 2.4f | SEM photograph of a center tap with initial barrier of 53 μm etched for 8 minutes | 18 |
| Figure 2.4g | SEM photograph of a center tap with initial barrier of 17 μm etched for 8 minutes | 19 |

| | | |
|---|---|---|
| Figure 2.4h | SEM photograph of a center tap with initial barrier of 51 μm etched for 4 minutes | 19 |
| Figure 2.5 | Etched distance versus time with all center taps formed with 25 different barrier sizes | 20 |
| Figure 2.6 | Individual center tap etched distance with specific barrier sizes | 21 |
| Figure 2.7 | Etched distance versus etch time for every 10 μm barrier size difference | 23 |
| Figure 2.8 | The resulting center tap at different etch times | 24 |
| Figure 2.9 | Etched distance versus barrier sizes at given etch times | 26 |
| Figure 2.10a | The design of a center tap with different etch rates | 29 |
| Figure 2.10b | End view of a center tap in a v-groove waveguide | 29 |
| Figure 2.11a | Etched distance versus barrier sizes at etch times of 8 and 12 minutes | 33 |
| Figure 2.11b | Design curve for tapping ratio versus barrier size at given etch times | 33 |
| Figure 3.1a | Masking patterns for a center tap | 36 |
| Figure 3.1b | The improved masking patterns for a center tap | 38 |
| Figure 3.2 | Final masking patterns for a center tap | 38 |
| Figure 3.3 | SEM photograph of a ruined center tap | 39 |
| Figure 3.4 | Fabrication of a center tap in a waveguide (Side View) | 41 |
| Figure 3.5 | Highlighted fabrication procedures for a center tap (Top View) | 42 |
| Figure 4.1 | Measurement setup for taps in the waveguide | 50 |
| Figure 4.2 | Scattering loss measurement with fiber probe for waveguide with taps formed by barrier sizes of 5 to 13 μm | 53 |

Figure 4.3 Scattering loss measurement with fiber probe for waveguide with taps formed by barrier sizes of 15 to 23 μm 54

Figure 4.4 Scattering loss measurement with fiber probe for waveguide with taps formed by barrier sizes of 25 to 33 μm 55

Figure 4.5 Scattering loss measurement with fiber probe for waveguide with taps formed by barrier sizes of 35 to 43 μm 56

Figure 4.6 Scattering loss measurement with fiber probe for waveguide with taps formed by barrier sizes of 45 to 53 μm 57

Figure 4.7 Tapping and attenuation in a waveguide 60

Figure b The end view of the polymer filled v-groove channel waveguide with center tap 76

## List of Symbols

| | |
|---|---|
| $\alpha$ | waveguide transmission loss in dB/cm |
| A | waveguide attenuation factor |
| $a_{eff}$ | effective waveguide transmission loss in dB/cm |
| e(t) | etched distance in μm |
| g | barrier size on the top of the wafer surface in μm |
| H | v-groove depth in μm |
| h(t) | tap height in μm |
| k | depression in polymer in μm |
| L | separation between taps in cm |
| P | tapped power in dB |
| R | vertical etch rate in μm/min |
| r | tapping ratio |
| t | etch time in min or tap width in μm |
| W | waveguide width in μm |
| x | tap position in cm |

## List of Nomenclature or Abbreviations

| | |
|---|---|
| AMC | Alberta Microelectronic Center |
| BOE | Buffered oxide etch |
| CVD | Chemical vapor deposition |
| EDP | Ethylenediamine Pyrocatechol |
| JFET | Junction field effect transistor |
| LIA | Lock-in-amplifier |
| NA | numerical aperture |
| NOA | Norland optical adhesive |
| OEICs | Optoelectronic integrated circuits |
| PCB | Printed circuit board |
| RIE | Reactive ion etching |
| SEM | Scanning electron microscope |
| TRLabs | Telecommunication Research Laboratories |
| UV | Ultraviolet |
| VLSI | Very large scale integrated |

# Chapter 1. Introduction

## 1.1. History and applications of optoelectronic integrated circuits

The problems associated with very large scale integrated (VLSI) circuits utilizing electrons as the carrier of information continue to increase with advancing system speeds [1]. At frequencies greater than 1 GHz, resistance in the electrical connections causes excessive heating and loss of signal power. This limits the number of output points to which the signals can be distributed, a situation referred to as low fanout. In addition, two or more closely spaced electrical wires in highly packed VLSI circuits may induce crosstalk with one another. On the other hand, loss in optical interconnections does not depend on the modulation frequency; hence, circuit heating and low fanout are not problems. Furthermore, optical interconnections are highly immune to crosstalk in dense circuits. They offer circuit designers an opportunity to pack data channels much closer without incurring increased throughput delays and system noise characteristic of high speed electrical interconnects. Therefore, the need for higher speed and better performance in VLSI circuits has prompted researchers to exploit light as the carrier of information.

The optical integrated circuit, the optical equivalent to the integrated circuit in electronics, was proposed by S.E. Miller of Bell Laboratories [2]. An optical integrated circuit is a thin film device which integrates optical components (for example, lens, gratings, and optical waveguides) on a single substrate. Integration of the optical elements helps in reducing the alignment difficulties for optical signal transmission. The next step is to integrate optoelectronic devices (for example, lasers and photodetectors) with optical circuits so that the signal can be processed electrically and transmitted optically. These circuits are called optoelectronic

integrated circuits (OEICs). Such circuits will eventually replace all-electronic signal processing circuits and will provide the interface between signal processing boards and optical fiber links.

OEICs are classified into two types: monolithic and hybrid. The monolithic type has various components such as lasers, optical waveguides and photodetectors, fabricated from the same material as the substrate. In hybrid OEICs, discrete optoelectronic devices are surface-mounted on a common substrate and are connected by integrated optical waveguides [3]. Although the monolithic OEIC is expected to be more reliable, implementation of all components on the same material is difficult. The hybrid OEIC, on the other hand, has the advantage of utilizing optimized discrete components [4]. Different applications of OEICs have been studied [5].

One device that can be realized in an OEIC is the optoelectronic switch matrix, a 10 x 10 version of which has been built at Telecommunication Research Laboratories (TRLabs) [6]. At present, the optical distribution system uses 100 optical fibers. However, the preparation of 100 optical fibers is time-consuming and expensive; the fibers are also fragile and take up a lot of space. One of the projects at TRLabs is to fabricate an integrated version of the 10 x 10 optoelectronic switch matrix.

The basic schematic of the OEIC switch matrix utilizing out-of-plane optical waveguide taps as optical interconnections is shown in Figure 1.1. An optical signal is launched into each waveguide, and each tap in the waveguide taps a fraction of the signal out-of-plane. A photodetector, which can be turned on or off individually by controlling its bias voltage, is positioned over each tap to collect optically distributed signal. The signals from all the photodetectors in a column are summed to give an output. In this way, the switch matrix can route information from any of the inputs to

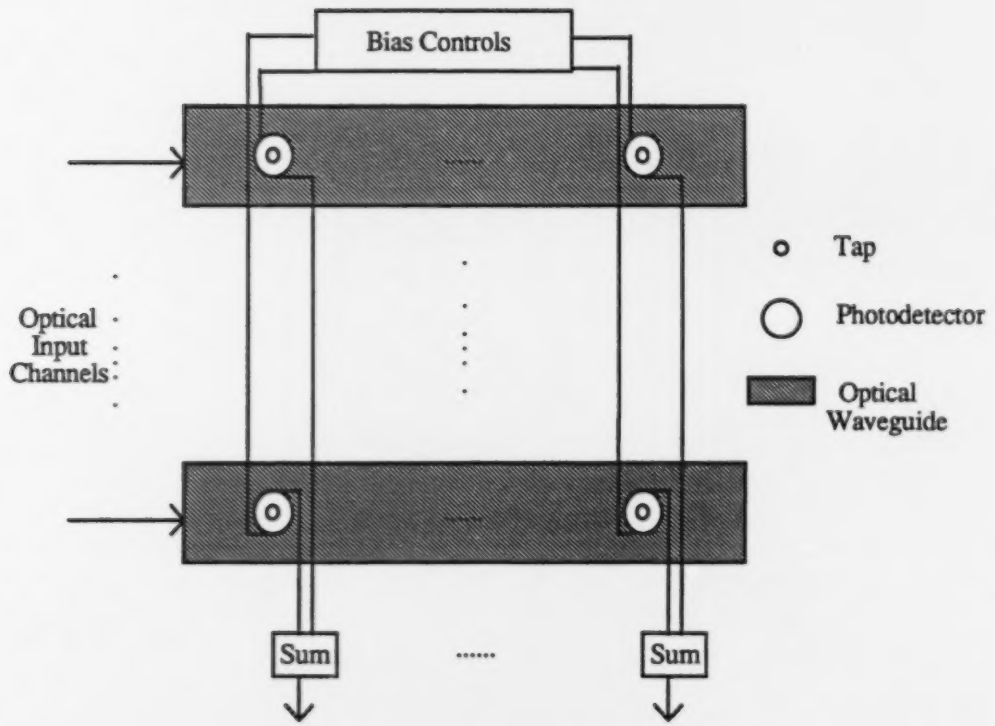


Figure 1.1 The schematic of OEIC switch matrix with optical waveguides and out-of-plane taps

any of the outputs. The subject of this thesis is the fabrication of out-of-plane taps in integrated optical waveguides.

### 1.2. Waveguides in OEICs

The integration levels of optoelectronic components are continually increasing to meet demanding applications in telecommunications and especially data communications. Optical waveguides can be considered the bond for integrating diverse components such as lasers, detectors, fibers, etc. in a single module. As in the optoelectronic switch matrix, the optical waveguide is one of the key components of any OEIC.

There are basically two types of planar optical waveguides on semiconductor substrates classified by the core position relative to the substrate; they are the ridge and channel waveguides. Each provides both vertical and lateral confinement. Waveguides with the core on top of the substrate are called ridge waveguides. Waveguides with the core buried in the substrate are called channel waveguides. "High silica" waveguides on silicon substrates, a commonly used type of ridge waveguide, have been extensively studied [7, 8]. However, out-of-plane coupling, which is required in hybrid connections, is difficult for this kind of waveguide. On the other hand, silicon v-groove waveguides, a type of channel waveguide formed by preferential etching of silicon [9], have been shown to be capable of out-of-plane coupling [10, 11]. The advantages of this kind of waveguide are (a) it is symmetrically bounded by smooth crystal planes which is an important factor for low loss lightwave guiding; (b) the end facet at the end of the waveguide can be used for coupling light into and out of the v-grooves; (c) this waveguide technology is compatible with fiber alignment using silicon v-grooves.

As mentioned above, the end facet of the v-groove waveguide, a (111) plane at an angle of 54.7° with the (100) silicon wafer surface, can be used for reflecting light from waveguide to a photodetector located at the surface of the wafer [11]. Figure 1.2 shows how the light is tapped. When the light travels to the end of the waveguide, it impinges on the end facet and reflects up at about 20° from the normal to the top surface of the waveguide. Since the waveguide is filled with a dielectric of index of refraction near 1.5, the angle in air will be about 30° from the normal due to refraction. Three-dimensional integrated optics using end facet coupling from silicon v-grooves has been suggested [11]. However, such end facet coupling can only tap 100% of the light in the waveguide. There is a requirement for integrated taps for out-of-plane coupling with controllable tapping ratios to achieve uniform distribution of light to numerous components. This requirement has lead TRLabs to search for different tapping geometries to tap a controllable amount of light from discrete taps along a waveguide.

Kumar [10] has recently reported low-loss polymer multimode waveguides with integrated out-of-plane taps in silicon v-grooves. Norland 61 (an optical adhesive with refractive index n=1.56), silicon dioxide (n=1.456), and Norland 68 (n=1.54) are the materials for the core, the lower cladding, and the upper cladding respectively . The reported waveguide transmission loss is less than 1 dB/cm [10]. The next section describes Kumar's method for fabricating integrated taps in these waveguides.

### 1.3. An integrated out-of-plane tap

An integrated out-of-plane tap in a waveguide is basically a power splitter whose function is to extract a fraction of light from the waveguide upward while the remaining portion keeps traveling in the original direction in the waveguide. The out-

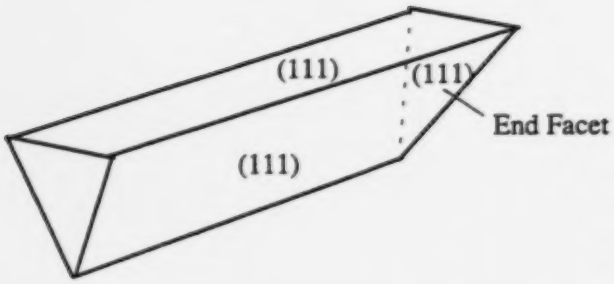


Three dimension view of a v-groove waveguide

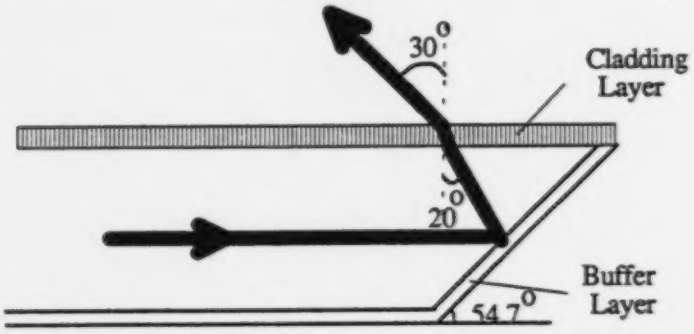


Side view of end facet tapping of waveguide

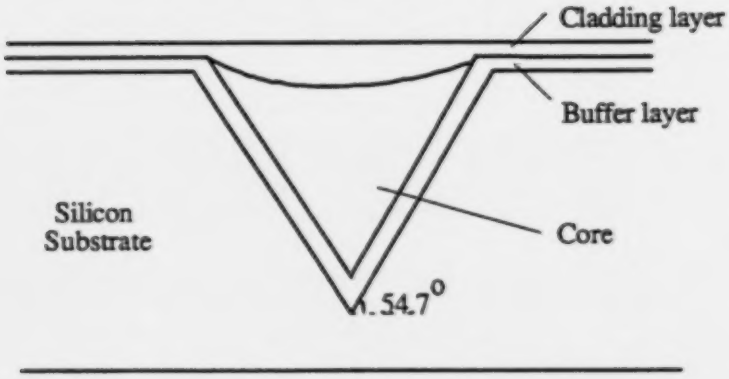


The end view of the v-groove waveguide

Figure 1.2 A v-groove waveguide with end facet tapping

of-plane sidewall tap developed by Kumar [10] uses an integrated reflector which can be fabricated anywhere along the waveguide and can be designed for specific tapping ratios. The reflecting plane in the waveguide is formed by a micromachining phenomenon called undercutting, which is one of the etching characteristics of silicon in Ethylenediamine Pyrocatechol (EDP) [12]. The fabrication procedures of this kind of tap are the same as that of the waveguide [10] and the reflecting plane is formed at the same time as the waveguide. Figures 1.3 and 1.4 show the mask pattern and final structure of a v-groove waveguide with one sidewall tap and an end facet. The plane of reflection of a sidewall tap is a (212) plane which intersects the (100) surface at 48.2° and whose trace makes an angle of 18.4° with the (111) trace [12]. The final tapping ratio can be controlled by the size of the rectangular mask projection.

Kumar has also fabricated a 12x12 tap array designed to provide equal reflected power at each tap [10]. However, this array did not perform as expected. The reason for this is that, occasionally, an unexpected plane other than the (212) plane appears during the chemical etching process of tap formation. This unexpected plane causes the light in the waveguide to deflect at a different angle. As a result, the detector at the designed location cannot collect all the tapped power. Other problems with sidewall taps are (a) the reflecting planes locate mainly on one side of the waveguide so that the light is reflected to the side and the photodetector will need to be located off the waveguide track to receive the light, and (b) the light reflected by the sidewall taps is at a different angle from that reflected by the end facet. These two factors may lead to complications in assembly. These problems indicate a need to produce an alternative form of out-of-plane tap which can tap out an arbitrary fraction of light from a waveguide without the problems associated with the sidewall taps.

In summary, low loss waveguides with out-of-plane taps are necessary components for coupling light to optoelectronic devices which are surface-mounted

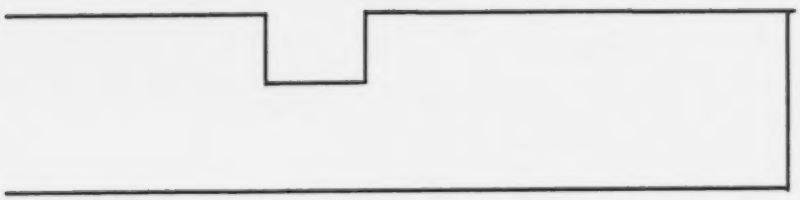

(a)

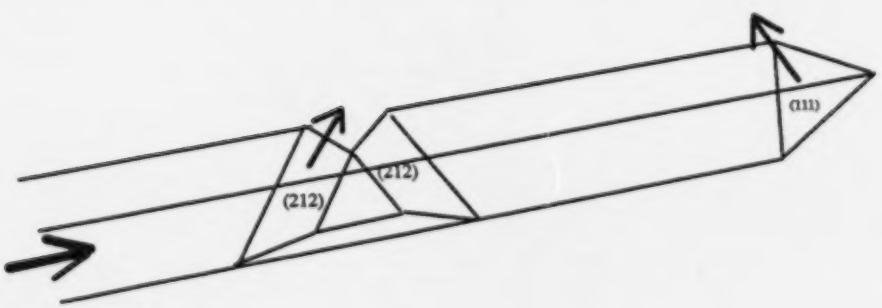


(b)

Figure 1.3 (a) Mask pattern for a v-groove waveguide with a sidewall tap and an end facet

(b) V-groove and sidewall tap and an end facet after EDP etching

using flip-chip technology. Applications of waveguides with taps exist in signal distribution and switching or signal processing technology. The development of integrated out-of-plane taps, the subject of this thesis, will be a useful contribution to hybrid OEIC technology.

### 1.4. Outline of Thesis

Chapter 2 introduces the development and design of a center tap. In this chapter, the etching mechanism and etching rate of the center tap have also been investigated. Chapter 3 describes the fabrication procedure of tapped waveguides. Chapter 4 presents the loss measurement setup, results and analysis of the tapped waveguides. Chapter 5 summarizes the work done and recommends areas for future work.

# Chapter 2. Design of Integrated Center Taps

## 2.1. The development of a center tap

A new tap has been conceived which is a modification of the smooth (111) end facet reflecting surface. Figure 2.1 shows the basic idea of this tap. Two v-groove waveguides located end-to-end with a small barrier in between are fabricated first. Next, a fraction of the end facet barrier is removed so that a portion of the light traveling in the waveguide will meet the reduced barrier and reflect upward, and the rest of the light which has no obstruction in its path will continue to travel in the waveguide. The fraction of light that is tapped is the ratio of the area of the reflecting surface to the cross-sectional area of the waveguide. This kind of tap is called a center tap for its physical location in the waveguide.

Different methods of reducing the height of the barrier were investigated.

(a) Reactive Ion Etching (RIE)

Reactive ion etching is a plasma-based dry etching technique which is a combination of physical sputtering with the chemical activity of reactive species. Compared to chemical etching, it is a faster and cleaner etching method compatible with automation. However, etch selectivity is much more difficult to achieve in RIE than in wet etching since substantial ion bombardment involved in RIE makes chemical differences between various materials less important in the etching process. All the unmasked silicon region will be etched to the same depth at the same etch time. For this reason, it is difficult to use RIE for fabricating taps with different tapping ratios in a single waveguide. Moreover, a surface roughening on the etched area, which is due to the ion bombardment on the wafer surface, is observed. This is undesirable because

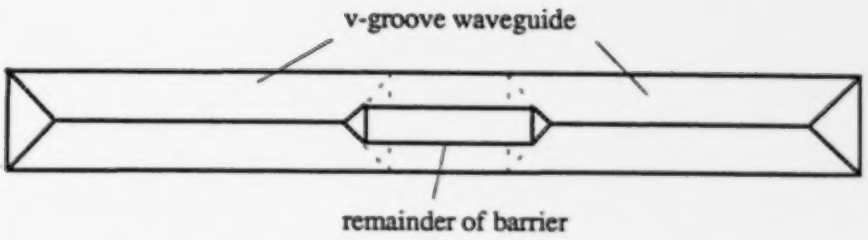


(a) Top View

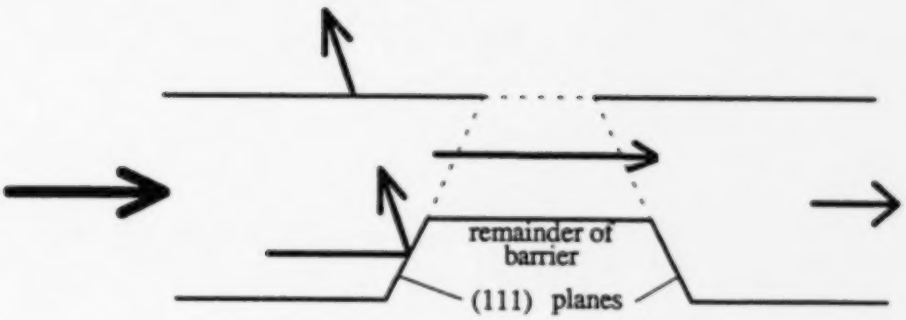


(b) Side View

Figure 2.1 The basic concept of a center tap in a waveguide.
Dotted line shows original barrier.
(a) top view (b) side view

the surface roughness on the reflector would scatter light in all directions and cause difficulty in capturing all the reflected light into the photodetector. Hence, RIE was not used to fabricate center taps.

(b) Anisotropic chemical etching with EDP

(i) Without removal of the masking material

Undercutting occurs when etchant removes material underneath the mask as in the method used by Kumar [10]. With the masking material still left on the barrier between the v-groove end facets, undercutting by EDP will eventually cause the two end facets to meet and etch down. Figure 2.2 shows the concept of using undercutting to achieve center tap formation. After the mask has been totally undercut, the barrier will be etched away. However, experiment showed that the undercutting rate is approximately 1 μm/h which is too slow and would cause difficulty in designing taps with specific tapping ratios.

(ii) Complete removal of the masking material

With the masking material on the barrier between the v-groove end facets completely removed before EDP etching, the etched barrier was expected to be as shown in Figure 2.1b. However, the etching of the barrier was observed to follow the outlines shown in Figure 2.3a. The upper surface of the barrier is two intersecting (112) planes which recede toward the bottom of the v-groove. An end view of the remaining barrier is shown in Figure 2.3b. The reflecting plane resulting from this method is a (112) plane, which has an angle of 35.3° with the (100) wafer surface. It was also observed that for a given etch time, the size of the barrier remaining depends on its initial size. It was evident that out-of-plane taps with specific tapping ratios could be designed with this etching method. To design center taps of arbitrary size, the etching mechanism and etch rate had to be better understood.

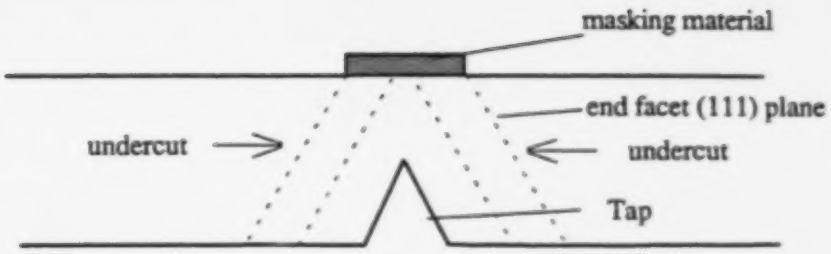


Figure 2.2 The concept of a center tap formation by undercutting

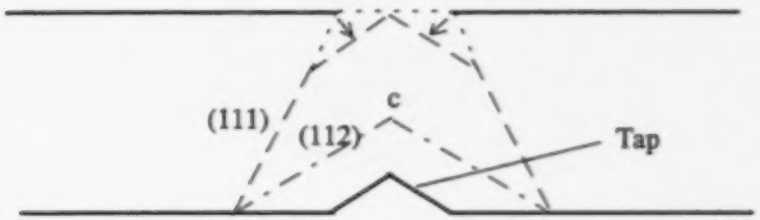


Figure 2.3a Observation of a center tap formation in EDP etching
Side View

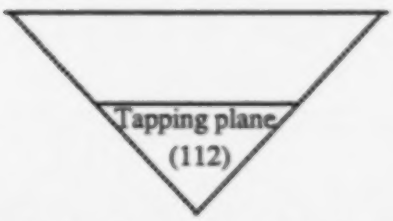


Figure 2.3b End view of a center tap in a v-groove waveguide

## 2.2. Determination of etch rate for center taps

To investigate the etching mechanism and to obtain the etching rates, experiments were done with a mask designed to produce 130 μm wide v-grooves with barriers of various sizes ranging from 5 μm to 53 μm in steps of 2 μm. (For details of the wafer processing, please refer to Chapter 3.) The center tap etching experiments were conducted after the $SiO_2$ mask on the barriers was removed. The wafer holder used can contain a maximum of seven samples. There were three identical sets of mask patterns with barrier sizes ranging from 5 μm to 53 μm on each wafer. In order to minimize any differences which may arise during fabrication, two wafers were processed at a time and each one was cleaved into three segments. The segments of one wafer were placed alternately with those of the other wafer on the holder. The holder with the six samples was put into the EDP solution so that all the samples would start etching at the same time. Every 4 minutes, a segment was removed from the EDP solution and examined. In this way, the etching observation results for 4, 8, 12, 16, 20 and 24 minutes with barrier sizes ranging from 5 to 53 μm were used to determine the etching mechanism and etching rate.

The fabricated center taps were viewed under an optical microscope. It was noticed that the maximum etch time for the formation of center taps with these barrier sizes is less than 20 minutes. Etching for 20 minutes completely removed the barriers and left only the waveguide. All the samples were examined under a scanning electron microscope (SEM) to inspect the center taps formed and to measure the etched depth. The etched depth of the center tap determines the size of the tapping surface, and hence the tapping ratio of the center tap.

The waveguide widths and the tap widths and lengths were measured. By simple geometric calculations, information on waveguide depth, tap height, and etched

distance can be obtained. By measuring the tap width and length in the SEM photographs, it was found that the tapping plane is (112). Typical qualities and sizes of the fabricated taps from different etch times are also shown in Figures 2.4a-h. After four minutes, the tapping surfaces consist of portions of (111) end facets and some unexpected planes. Therefore, the surfaces are rough. After eight minutes, the surfaces get smoother and the (111) end facets are etched away. After twelve minutes, the tapping surfaces are smooth but small. After sixteen minutes, the tapping surfaces become minute and most of the tapping barriers are completely etched. From the photographs, some details of the etching mechanism can be determined. In order to understand better the tap formation, the measured data are plotted in various ways for quantitative analysis.

The overall etched depth versus time for all samples with 25 different barrier sizes is plotted as shown in Figure 2.5. It can be seen that at any etch time, there is a variation in the etched distance which is due to the variation in barrier size among the samples. The etched depths versus time for six barrier sizes are shown in Figure 2.6. These six samples were chosen because (a) the barriers less than 39 μm were completely etched away at 16 minutes, and (b) information on the etched depth for the 41 and 51 μm barriers was not available at all the tested times because the barriers were irregularly shaped at some etch times. All six graphs in Figure 2.6 show consistency in etching characteristics. The etch rate of every four-minute interval varies. The general trend shows four stages of etching, fast-slow-fast-level off, at respective rates of approximately 6.5, 4, 10 and 2 μm/min. The remaining barriers after 12 minutes of etching are tiny and close to the bottom of the v-grooves. In general, the etched depth can be controlled by etch time. Hence, the area of the tapping surface can also be in turn controlled by the etching time.

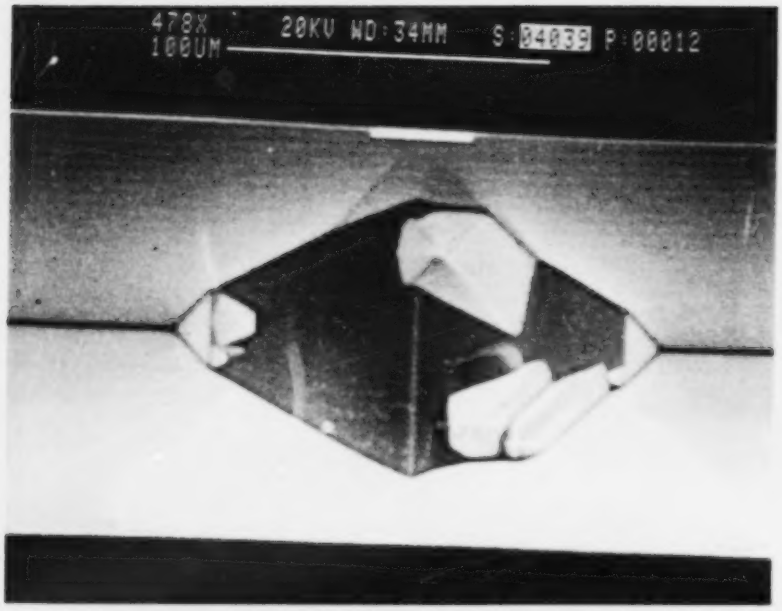


Figure 2.4a SEM photograph of a center tap with initial barrier of 39 μm etched for 4 minutes

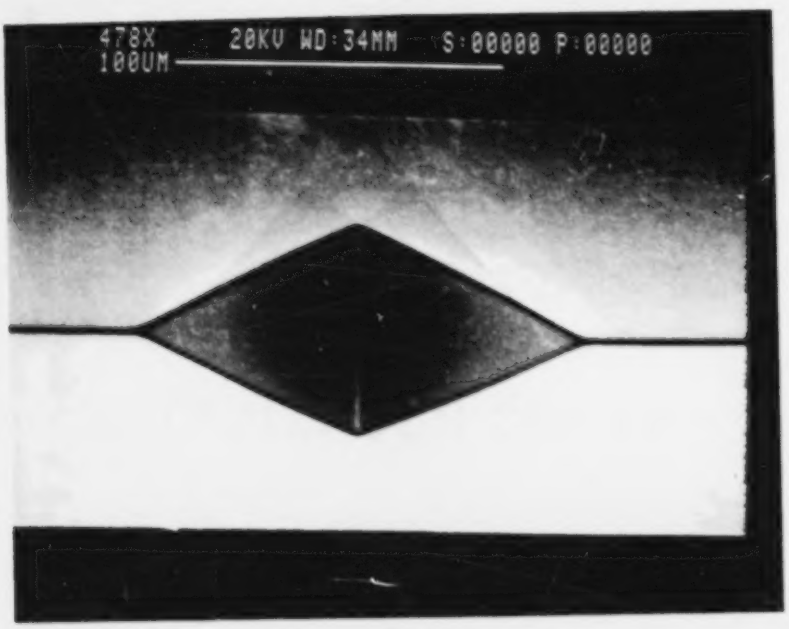


Figure 2.4b SEM photograph of a center tap with initial barrier of 39 μm etched for 8 minutes

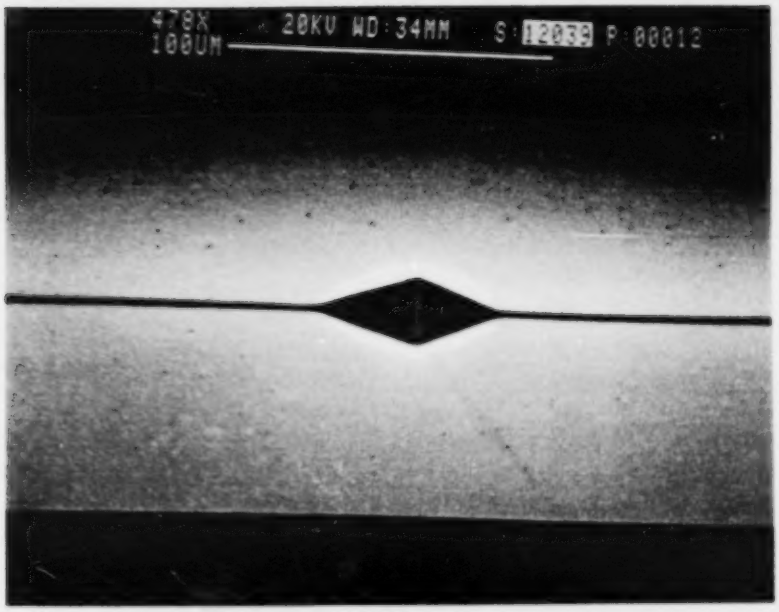


Figure 2.4c SEM photograph of a center tap with initial barrier of 39 μm etched for 12 minutes

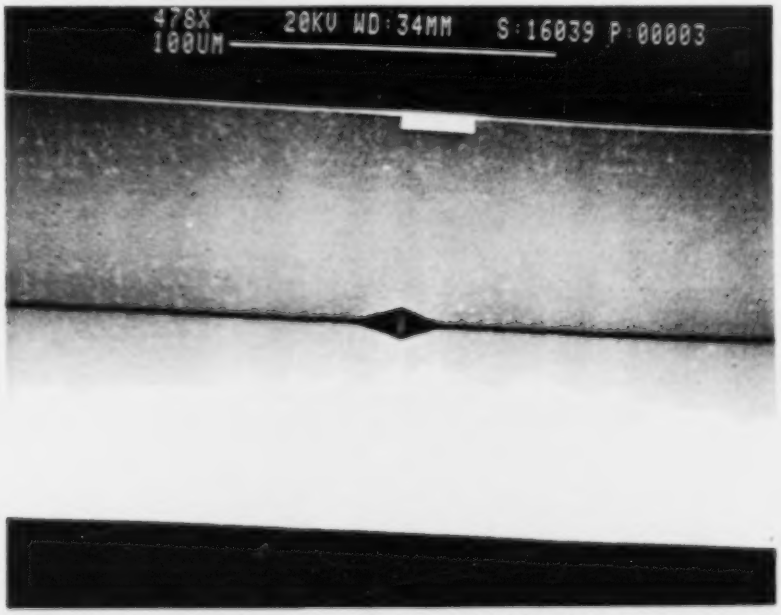


Figure 2.4d SEM photograph of a center tap with initial barrier of 39 μm etched for 16 minutes

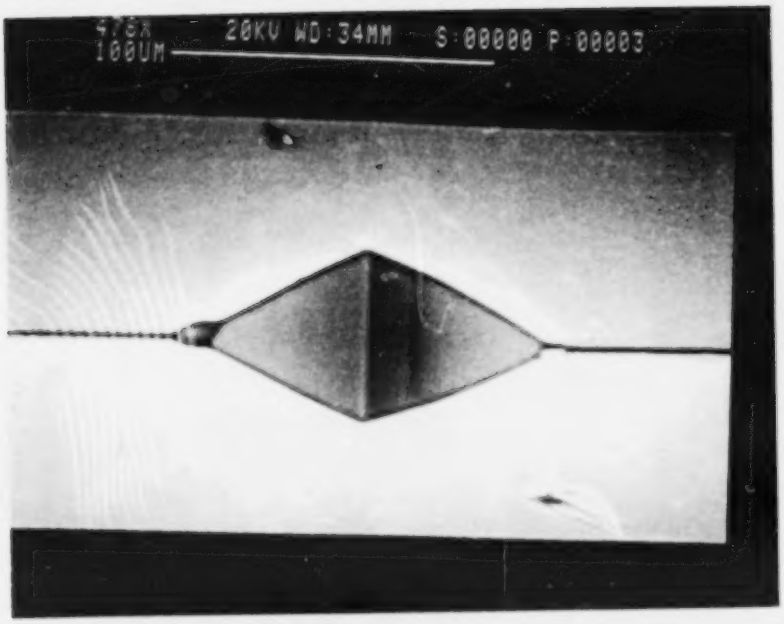


Figure 2.4e SEM photograph of a center tap with initial barrier of 5 μm etched for 8 minutes

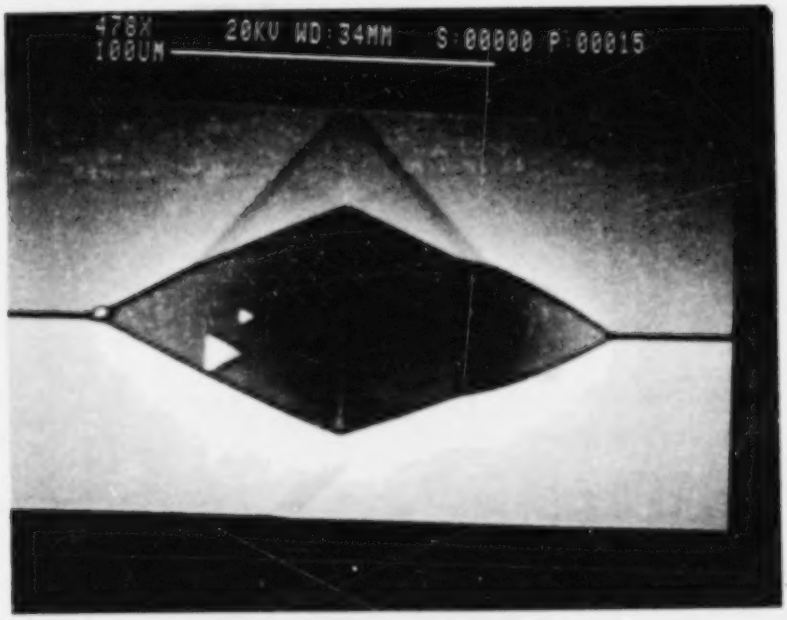


Figure 2.4f SEM photograph of a center tap with initial barrier of 53 μm etched for 8 minutes

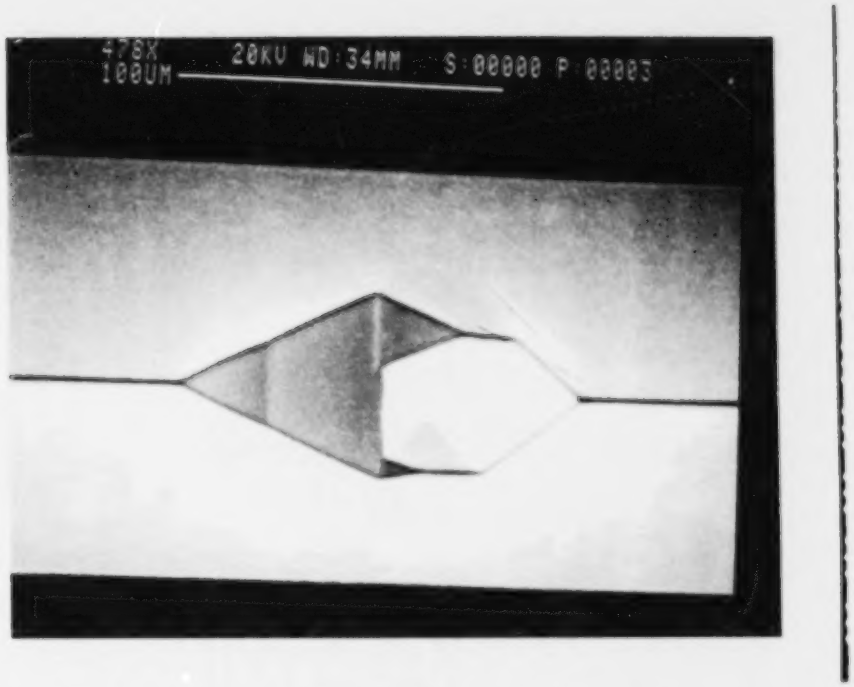


Figure 2.4g SEM photograph of a center tap with initial barrier of 17 μm etched for 8 minutes

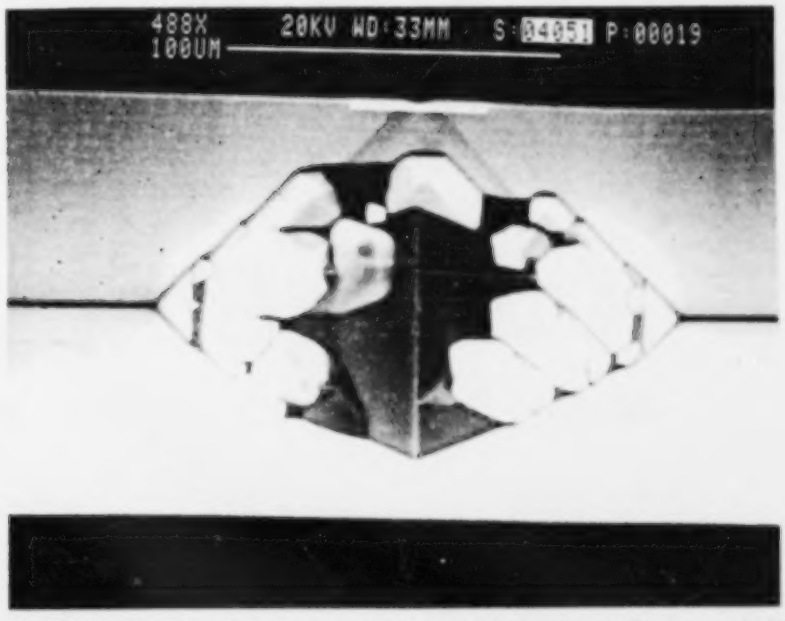


Figure 2.4h SEM photograph of a center tap with initial barrier of 51 μm etched for 4 minutes

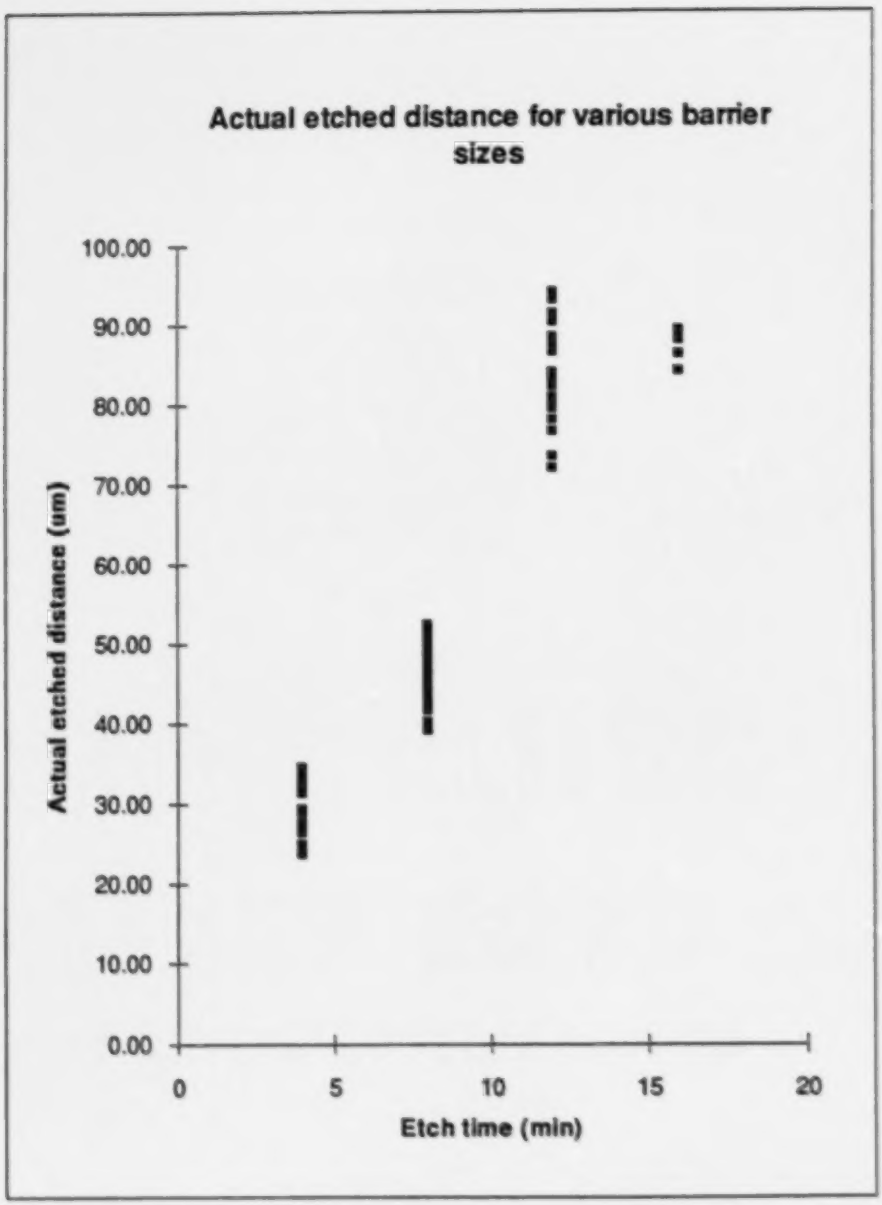


Figure 2.5 Etched distance versus time with all center taps formed with 25 different barrier sizes

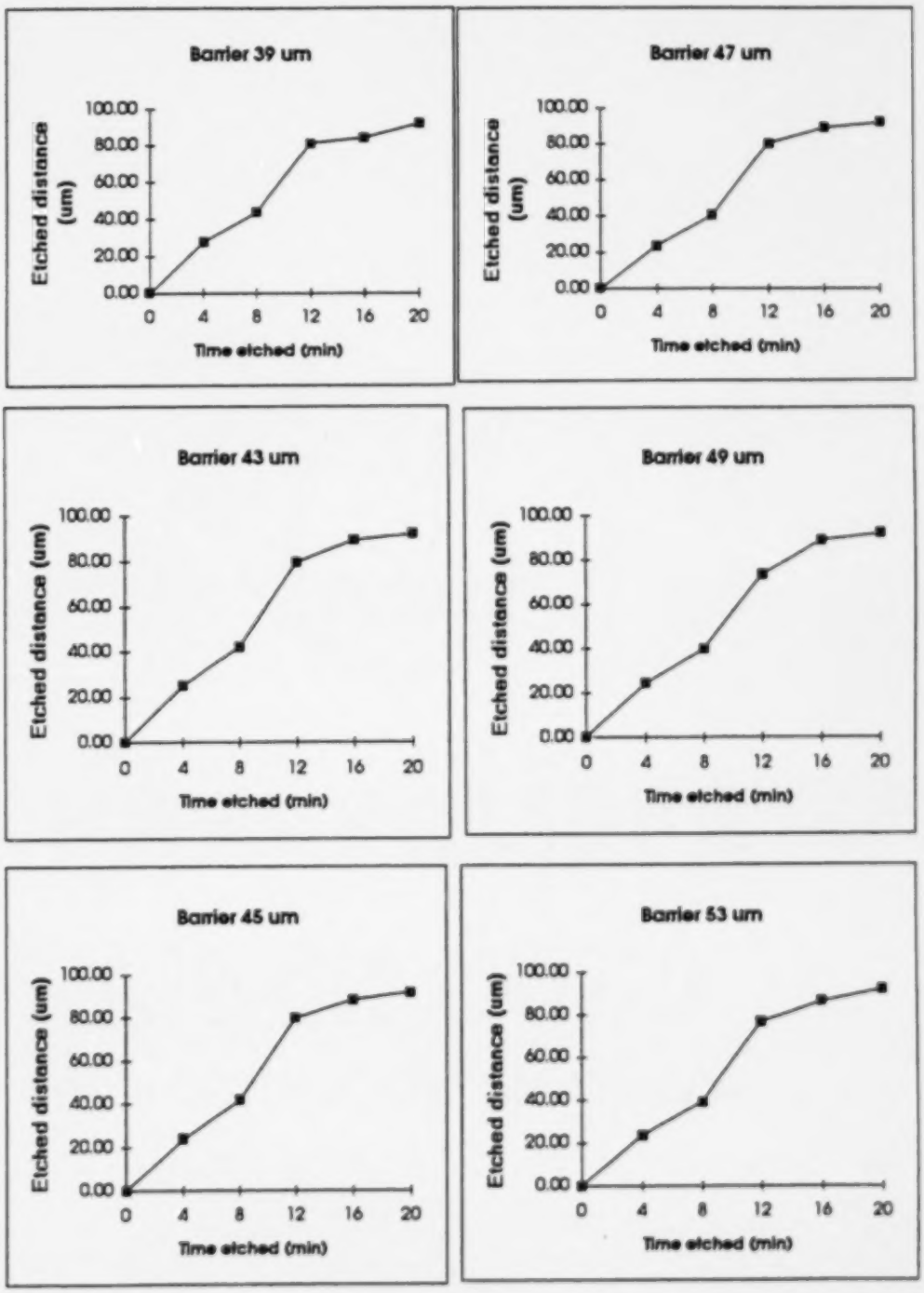


Figure 2.6 Individual center tap etched distance with specific barrier sizes

Figure 2.7 shows the etched depth versus etch time of the six different barrier sizes 9, 19, 29, 39, 49 and 53 μm. The first five plots are deliberately chosen to show the etch differences for barrier size difference of 10 μm. The plots show that the etch rate for the first four minutes for the smaller barriers is faster than for the bigger barriers, in particular, 9.0, 8.0, 7.5, 7.0, 6.6, and 6.0 μm/min for barriers of 9, 19, 29, 39, 49, and 53 μm respectively. This is expected since more etch time is needed for the two (112) planes of the bigger barriers to meet. At 16 minutes, the barriers of 9, 19 and 29 μm are completely etched. The etch rates for the rest of the samples are similar to the ones obtained in Figure 2.6.

Figure 2.8 summarizes the different stages of center tap formation and the corresponding etch time as deduced from SEM photographs in Figures 2.4a-h and the plots in Figure 2.6. After four minutes of etching, the top of the barrier has been etched away and the center tap has started to form. From 0 to 4 minutes, the downward etch rate varies from 6 to 9 μm/min. A rapid etching mechanism occurs in this short period of etching time. The etchant can attack the center tap from four directions. The tapping surface is a combination of crystal planes including small portions of the original (111) planes and is therefore very irregular. Etching is thus incomplete after the first four minutes. During the interval of 4 to 8 minutes, the etch rate slows down to approximately 4 μm/min. At eight minutes, the center tap surface roughness is reduced and the (111) planes have completely gone. The etching has passed through the point c (refer to Figure 2.8). However, some unexpected surfaces still exist. For the interval of 8 to 12 minutes, the etch rate increases to approximately 10 μm/min. At twelve minutes, the tapping surface is perfectly smooth and ideal for tapping. However, the tap sizes are small. The increased etch rate between eight and twelve minutes is possibly due to not having unexpected planes to be removed. After twelve

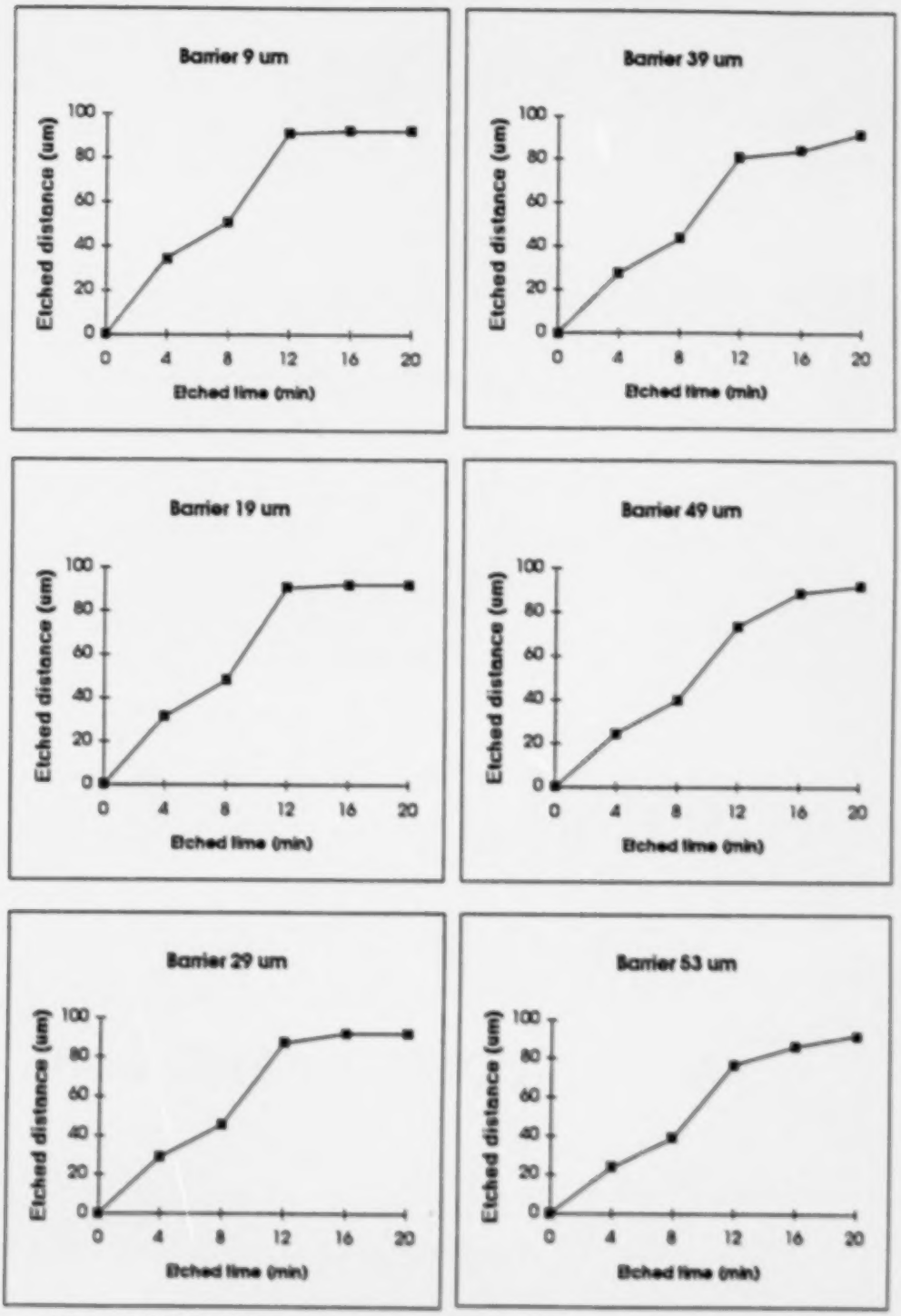


Figure 2.7 Etched distance versus etch time for every 10 um barrier size difference

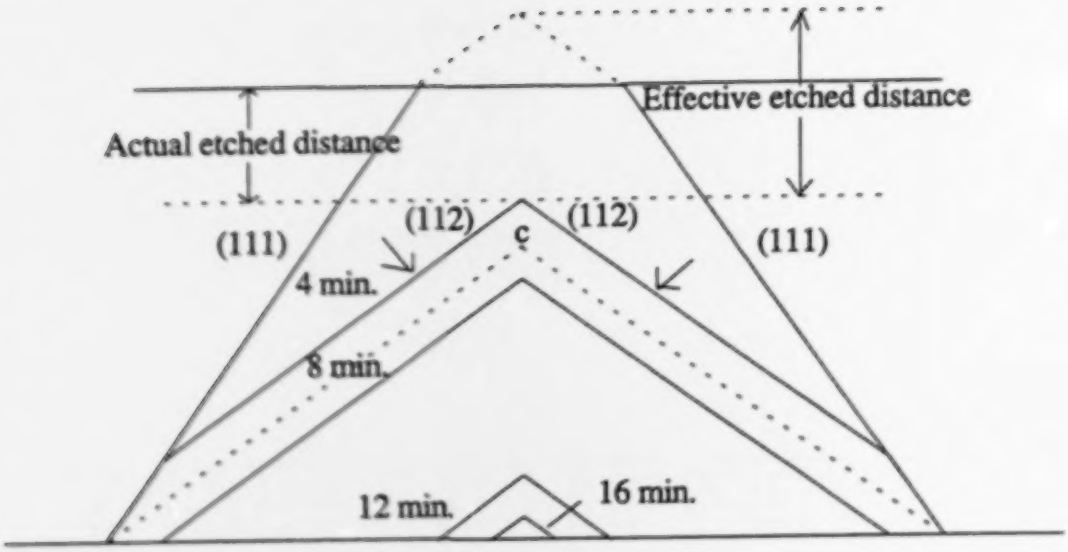


Figure 2.8 The resulting center tap at different etch times

minutes of etching, the etch rate levels off. The etch rate at the interval between 12 and 16 minutes is approximately 2 μm/min. A possible reason is that the etching solution may not be able to reach the bottom of the v-groove as easily. At 16 minutes, all samples with barriers less than 39 μm are completely etched away and the sizes of the remaining taps formed with barrier sizes greater than 39 μm are extremely tiny. At etch times of twenty minutes or longer, all barriers are completely etched away. The results of the experiments show that for barrier sizes between 5 and 53 μm, the proper etch time for these barrier sizes to form a reasonable tapping size is between eight to twelve minutes.

Another way to analyze the data is to plot etched distance versus barrier size for a given etch time. Figure 2.9 shows the actual and effective etched depth versus barrier sizes for a given etch time. The actual etched distance (refer to Figure 2.8) is the distance between the surface of the wafer and the tip of the remaining barrier. The effective etched distance is the difference between the height of the remaining barrier and the height the original barrier would have had were it bounded by two (112) planes as shown in Figure 2.8. This concept is used so that the first stage of etching can be thought of as a downward vertical etch.

The plots show that the actual etched distance decreases almost linearly as the barrier size increases. The fluctuation is due to fabrication error or measurement error. According to the etch results shown in Figure 2.9, the experimental equations obtained by least square fitting representing the relationship between the etched depth (or the tap height) and the barrier size at given etch times are as follows:

| | | |
|---|---|---|
| At 4 minutes, Actual | $e(4) = H - h(4) = 36 - 0.24g$ | μm |
| At 8 minutes, Actual | $e(8) = H - h(8) = 53 - 0.26g$ | μm |
| At 12 minutes, Actual | $e(12) = H - h(12) = 93 - 0.39\,g$ | μm |

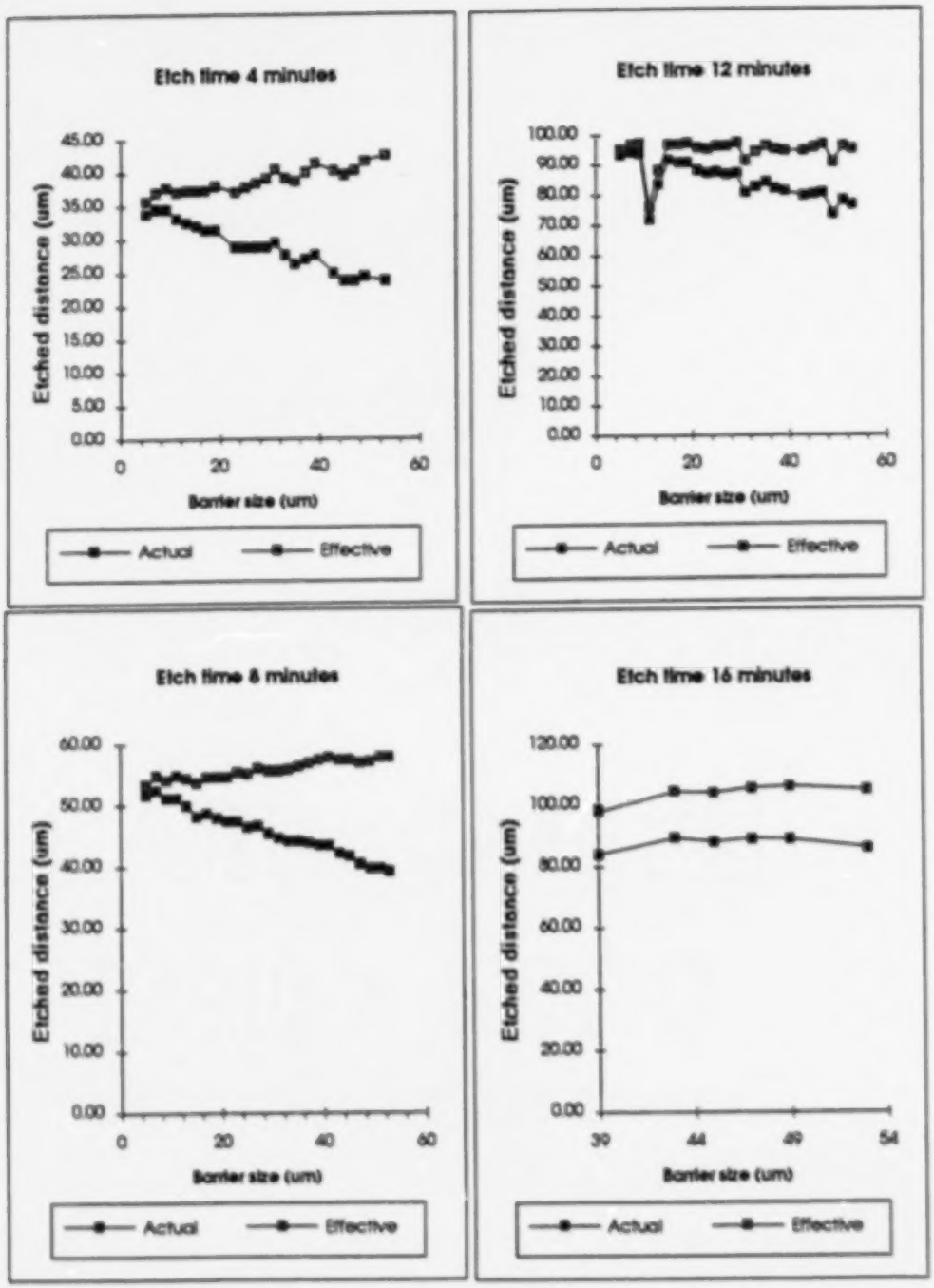


Figure 2.9 Etched distance versus barrier sizes at given etch times

At 4 minutes, the etched depth varies approximately 0.24 μm for every μm change in barrier size with an average etch rate of about 7.5 μm/min. At 8 minutes, the etched depth varies approximately 0.26 μm for every μm change in barrier size with an average etch rate of about 5.6 μm/min. At 12 minutes, the etched depth varies approximately 0.39 μm for every μm change in barrier size with an average etch rate of about 7 μm/min. At 16 minutes, there is not much difference in etch depth versus barrier size because the fabricated taps are too small. The average etch rate is about 5.5 μm/min. This shows that the barrier size can be used to control the final tap size.

The effective etched distance versus barrier size is almost flat with etched depths of approximately 40, 56, 96 and 104 μm at etch times 4, 8, 12, 16 minutes respectively. This indicates that the effective etched distance mainly depends on the etch time and that the barrier size has little effect on the effective etched distance. The average etch rates calculated from effective etched distances at times 4, 8, 12, and 16 minutes are 10, 7, 8 and 6.5 μm/min respectively. The differential etch rates calculated from the effective etch distances at the 4-minute etch time intervals are 4, 10, and 2 μm/min at the interval of 4 to 8, 8 to 12, and 12 to 16 minutes respectively. These etch rates are the same as the ones obtained from Figures 2.6 and 2.7.

In summary, the experiment shows that the chemical etching method for (112) center taps is possible. This method is based on a non-self-limiting timed etch. The etching mechanism of this experiment can be described in four stages. In stage one, a rapid etching period from start to the point c in Figure 2.8 will usually result in a rough tapping surface. In stage two, the etch rate slows down probably because after point c is passed, the etchant only has two directions of etch. In stage three, beyond the point c, the etch rate goes up as the amount of material to be removed is decreased and a smooth surface is provided. In the final stage, the etch rate levels off for the etchant may not be able to reach the bottom of the v-groove. In general, the etch time

has more influence on the tap size formation than the barrier size does. For this tapping method, by controlling the barrier sizes and etching time, we can design taps with specific tapping ratios.

### 2.3. Design of a tap with a specified tapping ratio

In this section, we use the information learned in the etching experiments to determine a method for designing a center tap with a given tapping ratio. The design is based on the assumption that the light traveling in the v-groove waveguide is uniformly distributed so that there is no modal selection at the taps Therefore the tapped fraction is equal to the ratio of the geometric area of the tap as seen by the light to the waveguide cross-sectional area.

Assuming etch rates are constant at different stages, and comparing the design equation with the experimentally obtained equations (from the actual etched distance versus gap size in Figure 2.9), we can deduce the etch rates at different stages. Knowing the tap formation process and the etching rates at different stages, we can design the masking dimension required at a given etch time for a waveguide tap of arbitrary size.

Figure 2.10 helps to explain the derivation of the formula for designing a specific size of center tap and deriving different etch rates at different stages. $R_1$ can be postulated as the average vertical etch rate of the two (112) planes before they meet at the center of the barrier on the wafer surface. A way to visualize $R_1$ is to pretend that the initial barrier is bounded by two (112) planes which intersect at a distance $\frac{g}{2\sqrt{2}}$ above the surface. $R_2$ is the constant vertical etch rate in μm/min during the time that (111) planes still form part of the sides of the barrier. $R_3$ is the

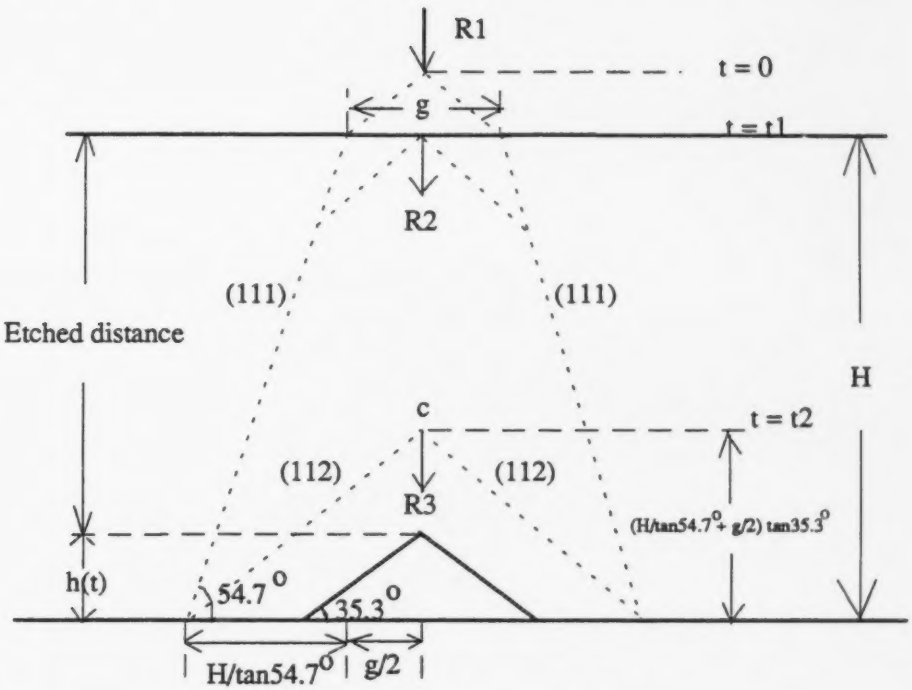


Figure 2.10a The design of a center tap with different etch rates

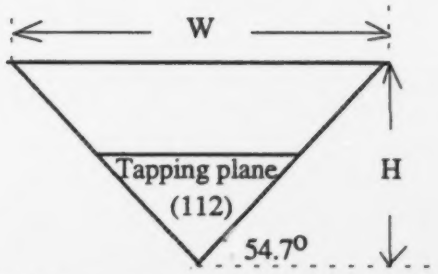


Figure 2.10b End view of a center tap in a v-groove waveguide

vertical etch rate in μm/min after the (111) planes have been completely etched away. Since the etch rates are assumed to be constants, they are simply the ratios of the etched distance in the vertical direction to the etch time. The etched distance can be determined by simple geometric calculation. The etch rates are found as follows.

Let h(t) be the barrier height in μm after t minutes of etching and let g be the original barrier width at the surface in μm. For a (111) v-groove, $H = \frac{W}{\sqrt{2}}$ is the waveguide depth in μm with W as the width of the waveguide in μm. For a waveguide of width W = 130 μm, the depth is H = 92 μm. The etched distance e(t) is H - h(t) in μm.

$t_1$ is the time for the two (112) planes to meet on the surface;

$$t_1 = \frac{g}{2\sqrt{2}R_1} \text{ min.} \qquad (2.1)$$

Since $t - t_1 = \frac{e(t)}{R_2}$ for $t_1 \le t \le t_2$,

the etched distance for $t \ge t_1$ is:

$$e(t) = R_2\, t - \frac{R_2}{2\sqrt{2}R_1} g \qquad \text{for } t_1 \le t \le t_2. \qquad (2.2)$$

Let $t = t_2$ be the etch time for the two (112) planes to recede to the bottom of the groove (the beginning of a center tap formation).

By simple geometry, we have

$$h(t_2) = \frac{H}{2} + \frac{g}{2\sqrt{2}} \qquad (2.3)$$

Substituting equation (2.3) into (2.2) at $t = t_2$ and rearranging, we get

$$t_2 = \frac{H}{2R_2} - \frac{g}{2\sqrt{2}}\left(\frac{1}{R_2} - \frac{1}{R_1}\right) \qquad (2.4)$$

As the etch time $t \geq t_2$, the etched distance becomes

$$e(t) = e(t_2) + R_3(t - t_2) \qquad \text{for } t \geq t_2 \qquad (2.5)$$

After manipulating, equation (2.5) becomes

$$e(t) = \left[R_3 t + \frac{H}{2}\left(1 - \frac{R_3}{R_2}\right)\right] - \frac{g}{2\sqrt{2}}\left[1 - \frac{R_3}{R_2} + \frac{R_3}{R_1}\right] \qquad \text{for } t \geq t_2 \qquad (2.6)$$

If this model is valid, the etch rates $R_1$, $R_2$ and $R_3$ can be deduced by comparing the coefficients of the theoretical etching equations with the experimental ones. According to the etch results shown in Figure 2.9, the experimental equations obtained by least square fitting representing the relationship between the etched depth (or the tap height) and the barrier size at given etch times are as follows:

At 4 minutes,

Actual $\qquad e(4) = H - h(4) = 36 - 0.24g \quad \mu m \qquad (2.7)$

At 8 minutes,

Actual $\qquad e(8) = H - h(8) = 53 - 0.26g \quad \mu m \qquad (2.8)$

At 12 minutes,

Actual $\qquad e(12) = H - h(12) = 93 - 0.39\,g \quad \mu m \qquad (2.9)$

By comparing equations (2.2) with (2.7), $R_1$ and $R_2$ are 13.1 μm/min and 8.93 μm/min respectively. With the obtained etch rates, $t_1$, $t_2$ and $h(t_2)$ can be calculated for different barrier sizes. For g varying from 5 to 53 μm, $t_1$, $t_2$ and $h(t_2)$ vary from 0.135 to 1.43 min, from 5.09 to 4.48 min, and 47.8 to 64.7 μm respectively. The values of $t_1$ and $t_2$ verify the observation from the experiment that the two (112) planes met in about a minute and the SEM picture shows that at 4 minutes' etch, small parts of (111) planes still form part of the sides of the barrier; therefore, $R_1$ and $R_2$

seem to be the right etch rates. However, comparing equations (2.6) with (2.8) or (2.9), $R_3$ values are inconsistent. Therefore, the postulation of constant $R_3$ is incorrect. This is also indicated in Figures 2.6 and 2.7. The assumption of constant $R_1$ and $R_2$ is not inconsistent with the data.

### 2.4. Design of taps in a waveguide with various tapping ratios

In some applications, the taps in a waveguide may be required to distribute different amounts of light and therefore must have different tapping ratios. With the etching characteristics of center taps observed in Section 2.2, the formation of taps with various tapping ratios in a single waveguide is possible. The objective is to have all different tap sizes (with the desired tapping ratios) formed at the same etch time. The key to designing various sizes of center taps in the waveguide is to utilize different sizes of the barriers to result in various tap sizes at the same etch time.

Figure 2.11a repeats the plots of actual etched distance versus barrier size at etch times of 8 and 12 minutes. To design the barrier size for the corresponding tapping ratios at etch times of 8 and 12 minutes, we convert the actual etched distance from Figure 2.11a to the theoretical tapping ratios using the equation described in Appendix B and plot the theoretical tapping ratio versus initial barrier size at given etch times in Figure 2.11b. Figure 2.11b shows that with barriers ranging from 5 to 53 μm, we can only achieve the tapping ratios of 0.25 to 0.45 for the etch time of 8 minutes and 0 to 0.05 for the etch time of 12 minutes. With these two experimentally obtained design curves, we can find the required barrier sizes for the desired tapping ratios at the given etch time. For example, if three center taps with ratios of 0.25, 0.35 and 0.45 are required, then the barriers would be 7, 27 and 47 μm respectively at an etch time of 8 minutes.

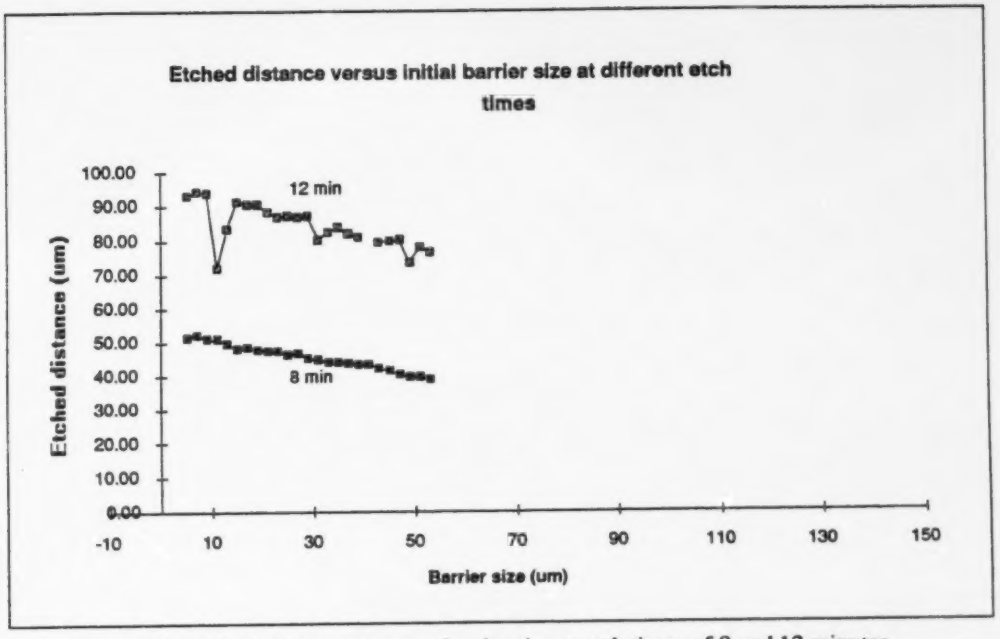


Figure 2.11a Etched distance versus barrier size at etch times of 8 and 12 minutes

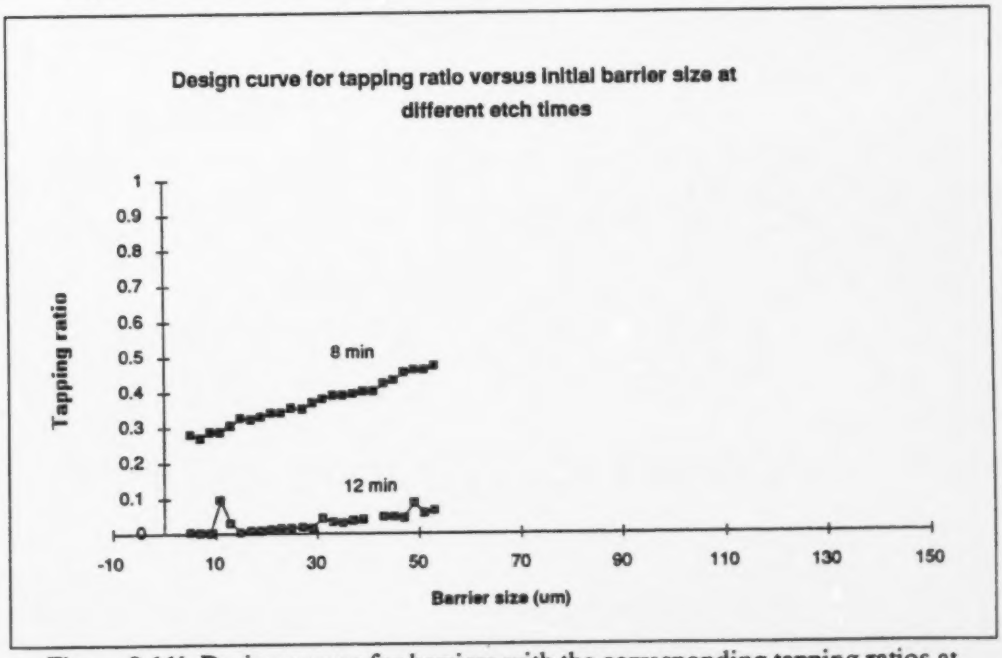


Figure 2.11b Design curves for barriers with the corresponding tapping ratios at different etch times

The experiments indicated that in order to have smooth tapping surfaces with reasonable tapping ratios, the etch time should be between 8 and 12 minutes. Therefore, experiments with etch times of 9, 10 and 11 minutes and with larger barrier sizes need to be done. The goal is to obtain at least one design curve which covers the full tapping ratio range of 0% to 100% for a single etch time.

# Chapter 3. Tap Fabrication

Center taps are fabricated by reducing the barrier formed by two end-to-end waveguides. Therefore, the key of fabricating a center tap is to selectively reduce the barrier in the waveguide.

## 3.1. Discovery of fabrication method, masking pattern and material

In the early fabrication development stage, the waveguide portions of the tapped waveguides were fabricated first by photolithography and anisotropic etching in EDP. Next, an attempt was made to pattern the small gap openings onto the locations between the two end facets of the waveguides. However, the photoresist used for patterning would not adhere to the wafer properly because most of the photoresist sank into the 90 μm deep v-grooves. Without a proper coating of photoresist on the required region of the wafer, the second pattern could not be transferred. As a result, a new fabrication procedure was developed for center taps.

Figure 3.1a shows the masking patterns for a center tap. The first pattern is to remove the masking material on the barrier before a second anisotropic etching. The second pattern is used to define the waveguides for the first anisotropic etching. After the patterns have been transferred onto the (100) silicon wafer, the v-groove channel waveguides were formed by dipping the wafer in EDP etchant for the first anisotropic etching in the fabrication process. Then the center taps can be formed in the second EDP etch after the removal of the oxide mask from the barriers. In the early development stage, the masking pattern pairs (refer to Figures 3.1a) were an exact match, that is, the gap size is exactly the same as the separation between two waveguide ends. However, this lead to an extremely difficult second pattern

First masking pattern for a center tap
(for tap region)

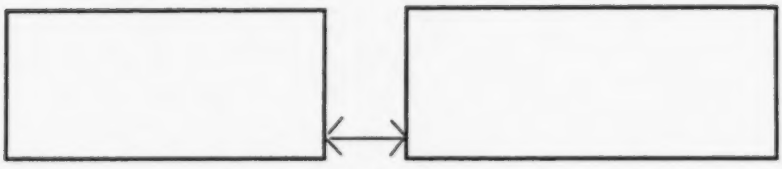


Second masking pattern for a center tap
(for v-groove waveguide formation)

Figure 3.1a Masking patterns for a center tap

alignment. Therefore, an additional 3 μm was added to both sides of the small gap pattern to ease the patterning alignment difficulty. Figure 3.1b shows the improved masking pattern for a center tap. Then there was another problem of incomplete removal of the masking material over the barriers. This was apparently due to the surface tension of the etchant which prevented small areas of silicon from being etched. A further problem occurred with the metal films used for the second masking materials. Metal films of chromium (Cr~20 nm) and gold (Au~100 nm) were used as the second masking layer materials for the second pattern. However, a mask lifting problem occurred during the EDP etching and the use of Cr and Au was abandoned. Therefore, a new mask pattern pair was designed to solve these problems.

Figure 3.2 shows the final masking patterns for the center taps. There is a long rectangular opening as the first mask pattern and several shorter rectangular patterns with small separations as the second mask pattern. Since EDP etching solution has a much higher etching rate (~ 5000 times) in silicon than in silicon dioxide, thermally grown silicon dioxide was used as the masking material for both masking patterns in the EDP etching process. The method of selective etching of the barrier was to use two different thicknesses of silicon dioxide layers with a pair of masking patterns.

Alignments for both first and second patterns during photolithography are still critical. Sometimes, the crystal orientation of the primary flat of a wafer can be off by a few degrees. In this case, all the fabrication will be ruined and the tapping surface will be unpredictable, as shown in Figure 3.3. One way to solve this problem is to pattern the wafer with several circular spots using an optical microscope and then anisotropically etch the wafer in EDP solution (refer to Appendix A). The EDP will etch along the real crystal planes; hence, the center tap patterns can be aligned to these "home-made" alignment marks.

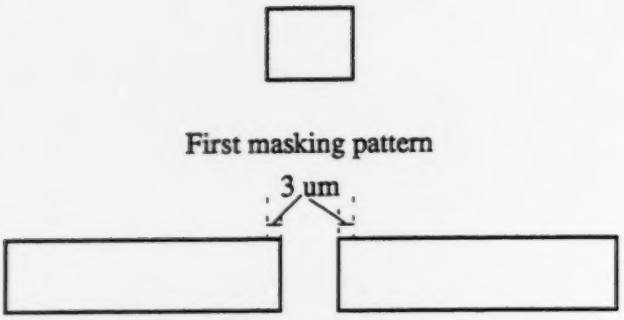


Figure 3.1b The improved masking patterns for a center tap

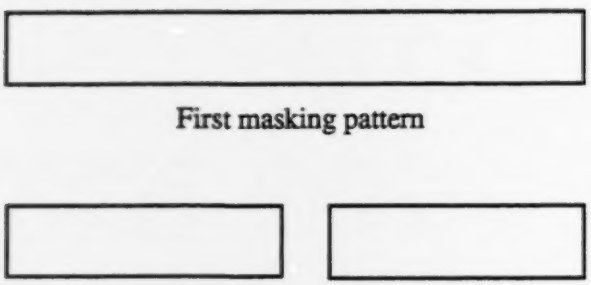


Figure 3.2 Final masking patterns for a center tap

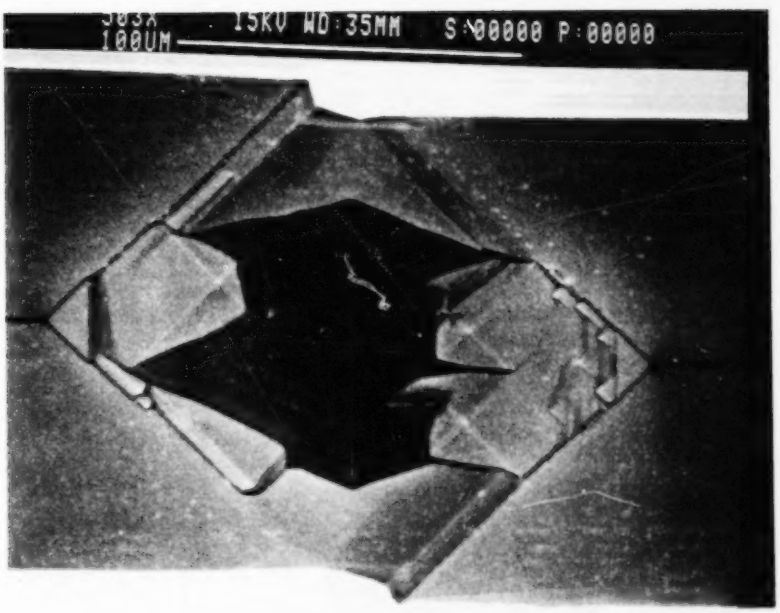


Figure 3.3 SEM photograph of a ruined center tap

Figure 3.4 shows the details of fabrication procedures of the center tap in the waveguide. Without any failure occurring in the fabrication, the whole fabrication process takes approximately one week. The procedures used in making waveguides with center taps are:

a. Photolithography (Figure 3.4 a-k, Figure 3.5 a-e)

b. Anisotropic etching (Figure 3.4 l-n, Figure 3.5 f-h)

c. Deposition of buffer layer of $SiO_2$ [13] (Figure 3.4 o)

d. Metallization of coupling planes [13] (Figure 3.4 p-t)

e. Application of core material [10]

f. Application of cladding [10]

g. End polishing for butt coupling [10]

Figure 3.5 highlights the key steps in fabricating a center tap. A first masking layer of silicon dioxide is deposited onto the (100) silicon wafer. Using the first masking pattern, the first layer of the silicon dioxide at the selected area is removed. A second layer of silicon dioxide is grown onto the whole wafer; the oxide layer at the region where the first pattern was will be thinner than the rest of the wafer. Then, the second masking pattern is transferred onto the wafer and the oxide at the specified region is removed so that silicon can be exposed. After the wafer is etched in EDP, the waveguide portions of the tapped waveguide is formed. Next, the thin layer of silicon dioxide between the waveguides formed is completely removed while the rest of the wafer is still protected by the oxide which was the thicker layer. Then, the wafer is etched in EDP again to reduce the barrier and the center tap is formed.

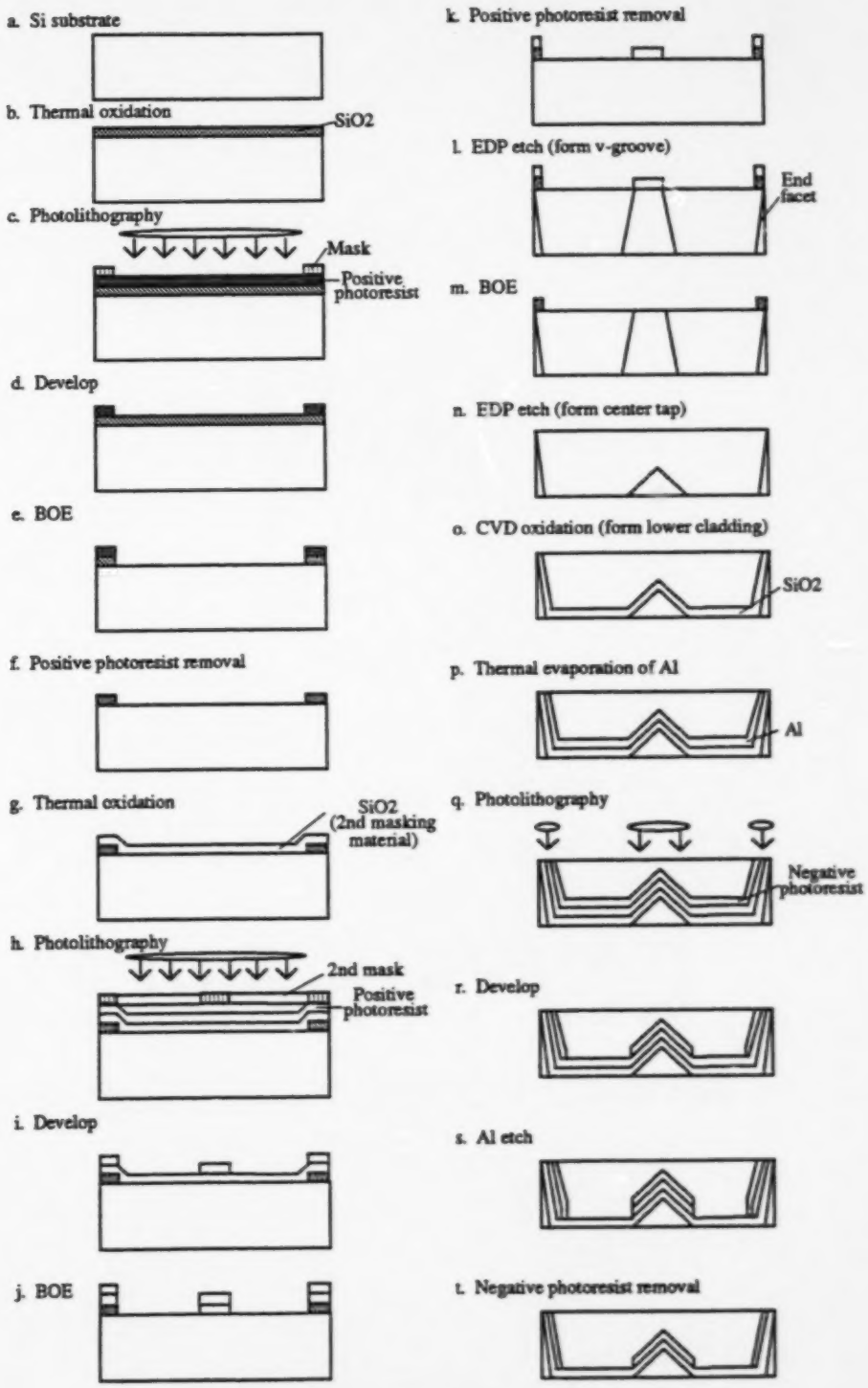


Figure 3.4 Fabrication of a center tap in a waveguide (Side View)

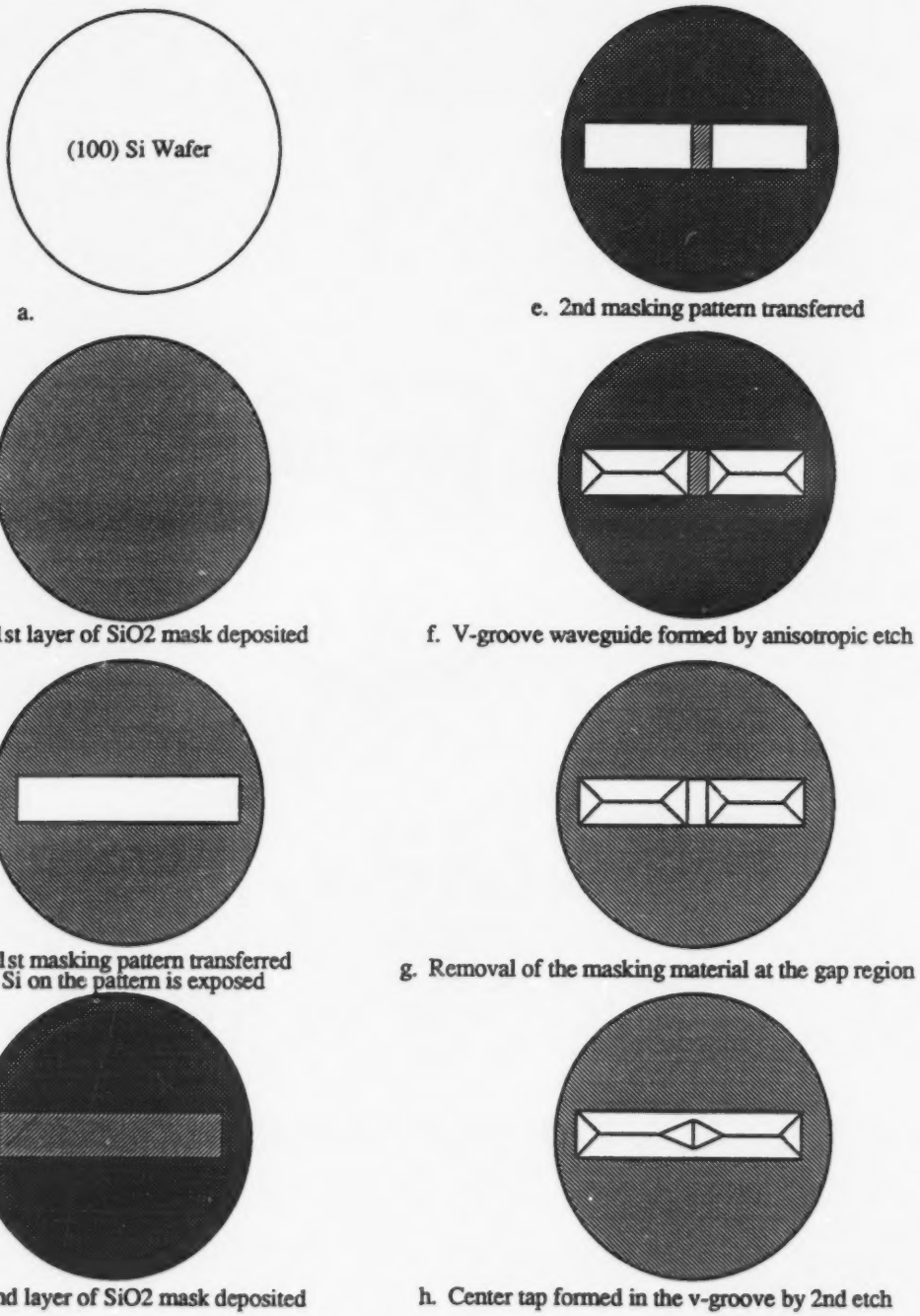
(100) Si Wafer
a.
b. 1st layer of SiO2 mask deposited
c. 1st masking pattern transferred
Si on the pattern is exposed
d. 2nd layer of SiO2 mask deposited
e. 2nd masking pattern transferred
f. V-groove waveguide formed by anisotropic etch
g. Removal of the masking material at the gap region
h. Center tap formed in the v-groove by 2nd etch

Figure 3.5 Highlighted fabrication procedures for a center tap (Top View)

### 3.2. Photolithography

Photolithography is the process of transferring a geometric pattern, which is required to selectively open the shape and area to be etched in the etching process, onto a wafer. The masking pattern pair will need two photolithography processes to transfer the patterns onto the wafer with two different thicknesses of oxide layers. Figures 3.4 a-k and 3.5 a-e show the detail and the highlight fabrication procedures for photolithography, respectively. The thickness of the first oxide layer is approximately 0.5 μm and the thickness of the second oxide layer is about 0.1 μm. After the second photolithography process, the oxide layer on the second pattern is completely removed and the region between the two end-to-end waveguides is protected by a thin oxide layer. The details of the process have been described by Kumar [10].

### 3.3. Anisotropic etching

An etchant which has a preferential etch rate in certain crystal orientation is called an anisotropic etchant. V-groove waveguides are defined by (111) crystal planes and center taps defined by (112) planes are formed by anisotropic etching of silicon.

Figure 3.4 l-n and Figure 3.5 f-h show the process described in this section. The anisotropic etchant EDP used in preferential etching of silicon is a mixture of ethylenediamine, pyrocatechol and deionized water. The mixing ratio is 750 mL ethylenediamine, 120 g catechol, and 240 mL deionized water. The higher atomic packing density in the <111> direction than that of the <100> makes the etching favorable in the <100> direction. EDP etches in the direction <100> about 35 times faster than in the direction of <111>. EDP etches in the <100> direction of silicon at a rate of approximately 0.6 μm/min and the silicon dioxide is etched at a rate of

approximately 0.2 nm/min. Thus, silicon dioxide can be used as a mask because of its resistance to etching by EDP.

Before EDP etching, a short dip of approximately 15 seconds in the buffered oxide etch (BOE) 10:1 solution to remove any native oxide formed on the exposed silicon regions is recommended. The wafer is held in a holder and put into the EDP solution kept in a reflux system when the solution temperature reaches 115°C. A magnetic stirrer driven by a external rotor is placed in the EDP solution to homogenize the etching solution. After being etched in EDP for 2.5 hours, the patterned locations on the wafer form v-groove waveguides which are defined by two smooth (111) sidewalls at an angle of 54.7° from the (100) surface. The wafer is then water cascaded for rinsing.

The thin second layer of silicon dioxide (~0.1 μm) located at the barrier between the end-to-end waveguides is removed in a BOE 10:1 solution for 5 minutes. The wafer is then dipped into the deionized water to rinse off the BOE and is put into the EDP solution for 8 to 12 minutes (or $t_2$ value as described in section 2.4) at 115° C. The wafer is again rinsed in the water cascade for half an hour. The silicon dioxide masking layer on the whole wafer is completely removed in BOE 10:1 solution for 7 minutes. The wafer is water cascaded for another half an hour and dried by nitrogen gas. Finally, the designed center tap size is fabricated and the wafer is cleaned for the next process.

### 3.4. Deposition of the lower cladding layer

The silicon substrate has a relatively high refractive index compared to the core material (optical adhesive). Therefore, a cladding layer is necessary to prevent refraction of the light from the core into the substrate. A 3 μm lower cladding layer of silicon dioxide is deposited using chemical vapor deposition (CVD).

### 3.5. Metallization of coupling planes

A tap is basically a reflecting plane to reflect light upward from the waveguide. A highly reflective tapping surface is essential for a high coupling efficiency. At optical wavelengths, a smooth silicon surface has a reflectivity of approximately 35%, which is not high enough to give efficient coupling. A reflectivity analysis on various metals at various wavelengths has been done at Alberta Microelectronic Center (AMC). The analysis shows that aluminum, compared to other metals, has the highest reflectivity of approximately 90%. Therefore, a 0.1 μm of aluminum film is deposited on the tapping surfaces to enhance the tapping reflectivity. There are many ways of aluminizing the tapping planes. For experimental purposes, we have chosen to use a manual way of metallizing the tap locations. This process was developed at AMC [13]. Figure 3.4 p-t shows the process of the selective aluminization of the tapping surface. Details of the process were described by Kumar [10].

### 3.6. Application of core material

Norland optical adhesive (NOA) 61 (with refractive index n=1.56) is the core material for the waveguide. It is dispensed using the squeezable container on the tapped waveguide regions of the wafer. A microscope glass slide is used to spread the adhesive uniformly on the wafer. The wafer is then kept in a vacuum jar at a pressure of -80 kPa for at least 5 minutes to remove any air bubbles which may be present in the adhesive. Next, a rubber sheet with a sharp edge is applied along the waveguide with adequate pressure to remove the excess liquid adhesive. This "doctorblading" of the polymer results in an extremely smooth concave depression surface of the adhesive in the v-groove due to surface tension (refer to the Figure b in Appendix B). The depression of the adhesive is about 20 μm for a 130 μm wide waveguide. The

adhesive is then cured under a 200 watts mercury lamp emitting 5 mJ/cm$^2$ for 20 minutes. Any excess cured polymer remaining on the surface can be removed using a 600 (particle size 14 μm) or 800 (particle size 9.5 μm) grit soft abrasive paper clamped on the wheel of a grinding/polishing machine with controllable rotation rate of 50 to 500 rpm. A smooth surface on the core is important for low loss waveguide transmission. The concave surface of the polymer prevents the abrasion of the core and maintains a smooth core surface. However, abrasion still roughens the edges of the waveguide which may cause scattering loss.

### 3.7. Application of cladding

A smooth surface cladding layer of NOA 68 (with refractive index n=1.54) may be used to reduce the scattering loss caused by the surface roughness of the waveguide and provides mechanical protection for the core material.

The sample is placed on the vacuum chuck of the spinner and the adhesive is dispensed from its container. The adhesive is viscous and is warmed to 50°C to reduce its viscosity in order to ease the spreading. As soon as the adhesive is poured on the sample, the spinner should be started. The spinning speed affects the thickness of the cladding; the higher the spinning speed, the thinner is the cladding layer. For a spin-on time of 15 seconds, a thickness of 55 μm is obtained at spin speed of 5000 rpm. The adhesive is then cured for 10 minutes under the ultraviolet (UV) lamp.

### 3.8. End polishing for butt coupling

Light is butt-coupled into the waveguide from a multimode fiber. A smooth input end surface of the waveguide can provide better coupling. This is achieved by grinding the sample end with a 400 grit (particle size 22 μm) abrasive paper clamped on a grinding machine with water lubricating the grinding surface and flushing away

the ground material until the input end of the waveguide is at the edge of the sample. It is followed by polishing the input end of the waveguide with a 1 μm mean roughness glass plate until the end is reflective. The end is then inspected under the microscope for flatness and smoothness.

# Chapter 4. Optical Properties of Waveguides with Center Taps

The optical properties of the fabricated waveguides that are of interest are the actual tapping ratios and the waveguide transmission loss. A side-scattering detection method was used to obtain scattered and reflected power from waveguides and taps. The quality of the fabricated center taps in the waveguides, such as smoothness and angle of the reflecting plane, can affect the tap performance. Therefore, depending on the fabrication quality, some mismatches between the measured and the predicted values of the tapping ratios and the waveguide loss are expected.

## 4.1. Introduction to the measurement method

The transmission loss in the tapped waveguides was determined by a side-scattering method [14, 15]. In this method, it is assumed that the scattered light intensity is proportional to the guided light intensity along the waveguide. A plastic optical fiber with a large numerical aperture (NA) was used as a probe to collect light scattered at 90° from the waveguide. The probe angle and the distance between the probe and the waveguide were maintained constant and the probe end was placed in proximity to the waveguide. The captured power was measured as a function of distance along the waveguide. The measurement accuracy is inversely proportional to the waveguide quality. Measurement of less than 1 dB/cm is difficult because the better the waveguide quality is, the less scattered power can be detected. Since our main interest is in the taps, the measurements were performed on aluminized v-groove waveguides with taps filled with polymer and without the upper cladding layer. This

simplified the processing while increasing the waveguide loss. It was hoped that the scattered power from the waveguides between taps could be directly observed. The advantage of this method is a non-destructive and non-contact measurement. Also, this method can be automated either by motorizing the probe along the waveguide or by capturing the image of the streak of light with a video camera. With an analog-to-digital converter, the information obtained from the video camera is converted into numbers, which can be stored and analyzed in a microcomputer [16].

### 4.2. Measurement setup

Figure 4.1 shows the measurement setup for the optical properties of tapped waveguides. Light emitted from a helium neon (HeNe) laser at the wavelength of 632.8 nm was focused through a lens into a multimode optical fiber which was butt-coupled to the input end of the waveguide. A beam chopper placed between the laser source and the lens, and a lock-in-amplifier (LIA), were used to minimize noise in the measurement caused by stray light. The chopping frequency of 200 Hz, set to avoid the harmonics of 60 Hz from the ac power supply, was fed into the LIA as the reference signal.

There was a limited number of samples to be used for measurement due to the difficulty and complication in the fabrication process. The samples fabricated with 8 minutes of etching from the etching experiment were used. Each sample contained 5 tapped waveguides. Each waveguide was 3 cm long with 5 center taps and 1 end facet separated by a distance of 0.5 cm. Therefore, taps formed from barriers of 5, 7, 9, 11, 13 μm were in one waveguide, 15 to 23 μm in the second, 25 to 33 μm in the third, 35 to 43 μm in the fourth, and 45 to 53 μm in the fifth. The tapped waveguides were aluminized and filled with Norland 61 as the core material.

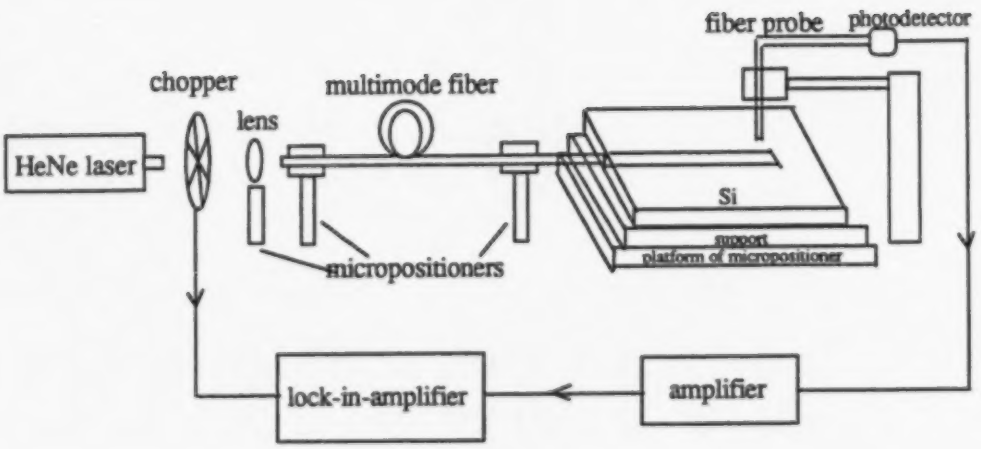


Figure 4.1 Measurement setup for taps in the waveguide

The sample was epoxied onto a piece of printed circuit board (PCB) substrate for support. The PCB was placed on the platform of the micropositioner which had 5 degrees of freedom, three translational and two rotational. Two alignments between the probe and the waveguide were done to provide measurement consistency along the waveguide. Since either the sample could be unevenly epoxied on the PCB or the platform could be tilted, a height adjustment between both ends of the waveguide was done to maintain a constant separation distance between the probe and the sample. The second alignment was a lateral adjustment to make sure that as the probe traveled along the waveguide, it would remain directly above the waveguide.

The plastic fiber (core diameter of 1 mm and NA of 0.5) used as a probe to collect the scattered light from the tapped waveguide had both ends polished, and delivered the captured light to a silicon photodetector (S-1087 Hamamatsu). The signal received by the photodetector was amplified 1000 times by a circuit containing a (junction field effect transistor) JFET-input op-amp and then fed into the LIA. The LIA gave an uncalibrated measurement readings of the scattered power.

The fiber probe was moved in steps of 0.5 mm and in finer steps of 0.02 mm near the tapping areas along the 3 cm long tapped waveguides and the readings were recorded. The readings from the LIA were converted into decibels and plotted against the probe distance in centimeters along the waveguide. The optical properties of the waveguides with center taps were evaluated based on these plots.

Other measurements were made by replacing the fiber probe with the photodetector so that more scattered power could be collected without being limited by the numerical aperture of the fiber. The photodetector was placed close to, but not touching, the wafer surface, and directly above each tap of the waveguide. The detected power was amplified and fed into the LIA as before. Only the power

reflected from the taps was measured this way in order to avoid the resolution problem.

### 4.3. Waveguide tap measurement results

In the absence of any coupling loss, defect or tap, a plot of collected power in dB versus the distance along waveguide in centimeters will be a straight line with a slope equal to the waveguide attenuation in units dB/cm. Coupling losses at the input to the guide will appear on the plot with a different slope, and defects and taps in the waveguides will appear as peaks in the data if they cause excess light to scatter out of the guides. In a waveguide with taps, the tapped power is orders of magnitude greater than the side-scattered power as will be seen below.

Figures 4.2-4.6 show the results of the scattering measurements using the fiber probe. At the tap locations, significant amounts of power have been tapped. The six distinctive scattered power peaks on each plot verify the out-of-plane tapping capability. Similar amounts of tapped power relative to the background side-scatter were measured from the five center taps along each waveguide. This is expected since all five taps along a single waveguide are similar in size. Also, it can be shown that the tapping surface has a direct influence on the tapping performance. For example, an abnormally high tapped power at the tap location with a 17 μm barrier size is shown in Figure 4.3. There is a huge unetched portion left on the tapping surface which increases the tapping area and hence the tapped power. From the plots, any deviation from the general trend corresponds to a peculiarly formed tapping surface. Only the end facet, which is a 100% tapping plane with a different angle of reflected light, has a higher tapped power relative to the background. It is also observed that the light from the end facet has a different shape of plot than the rest of the taps. This can be

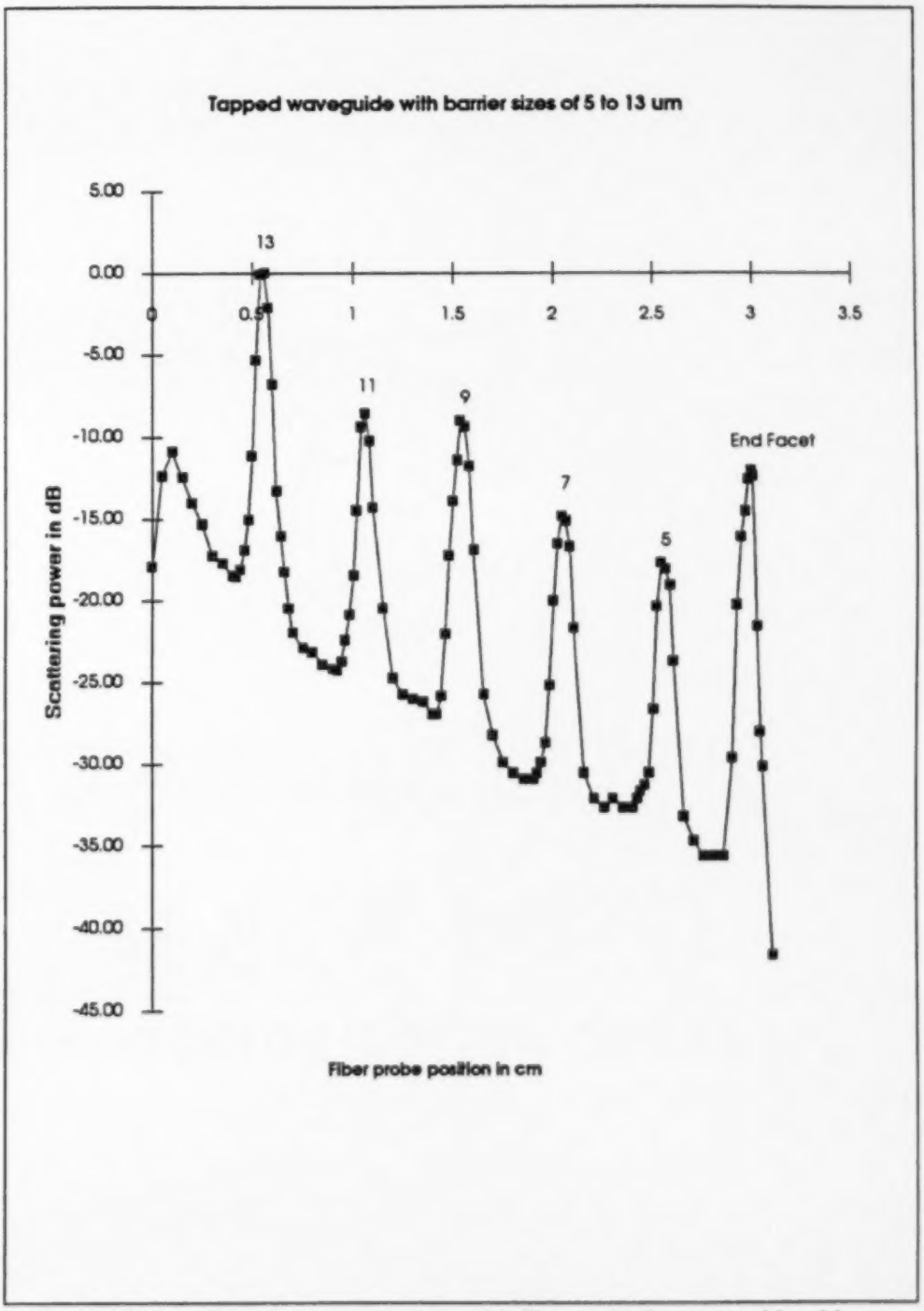


Figure 4.2 Scattering loss measurement with fiber probe for waveguide with taps formed by barrier sizes of 5 to 13 μm

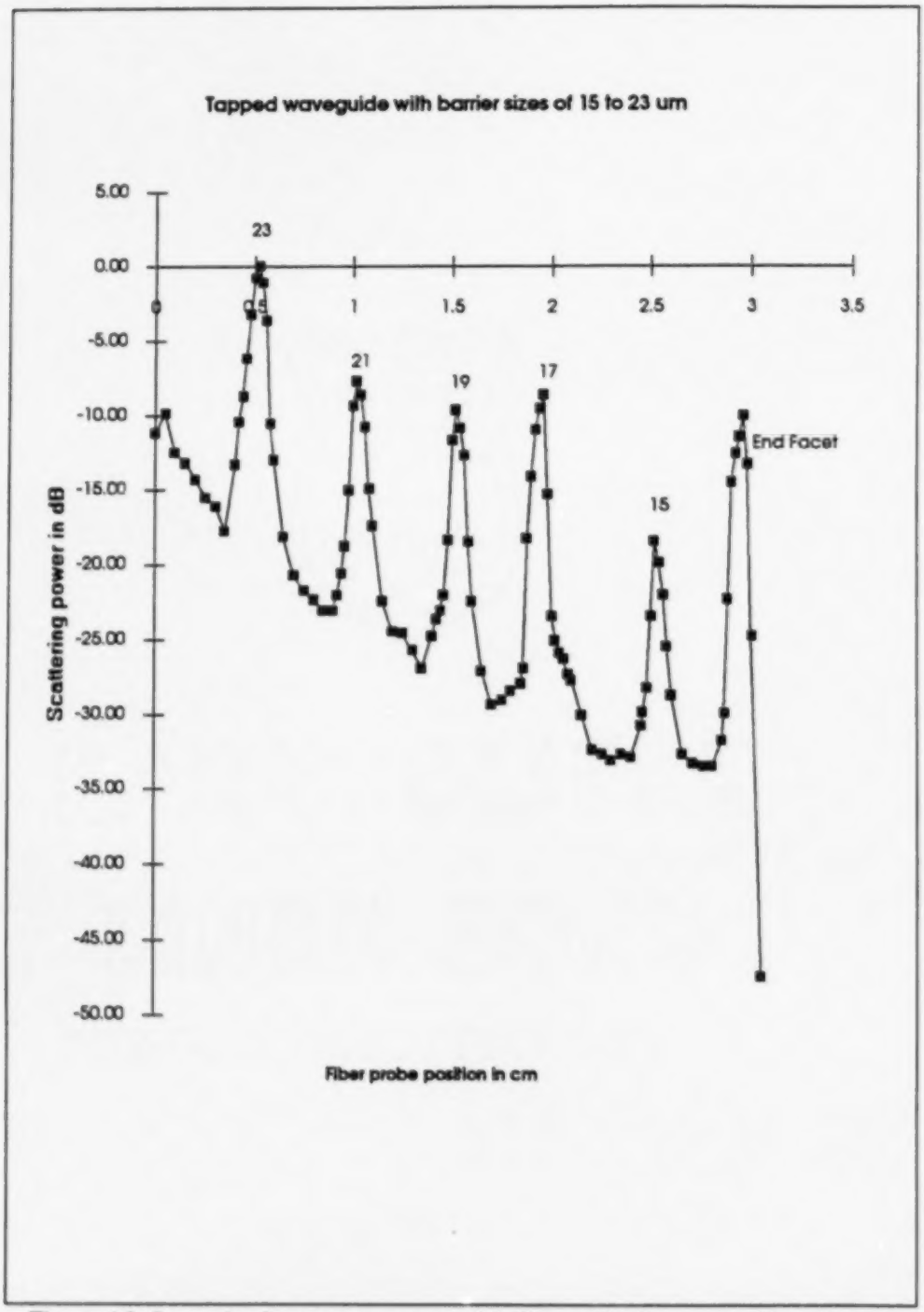


Figure 4.3 Scattering loss measurement with fiber probe for waveguide with taps formed by barrier sizes of 15 to 23 μm

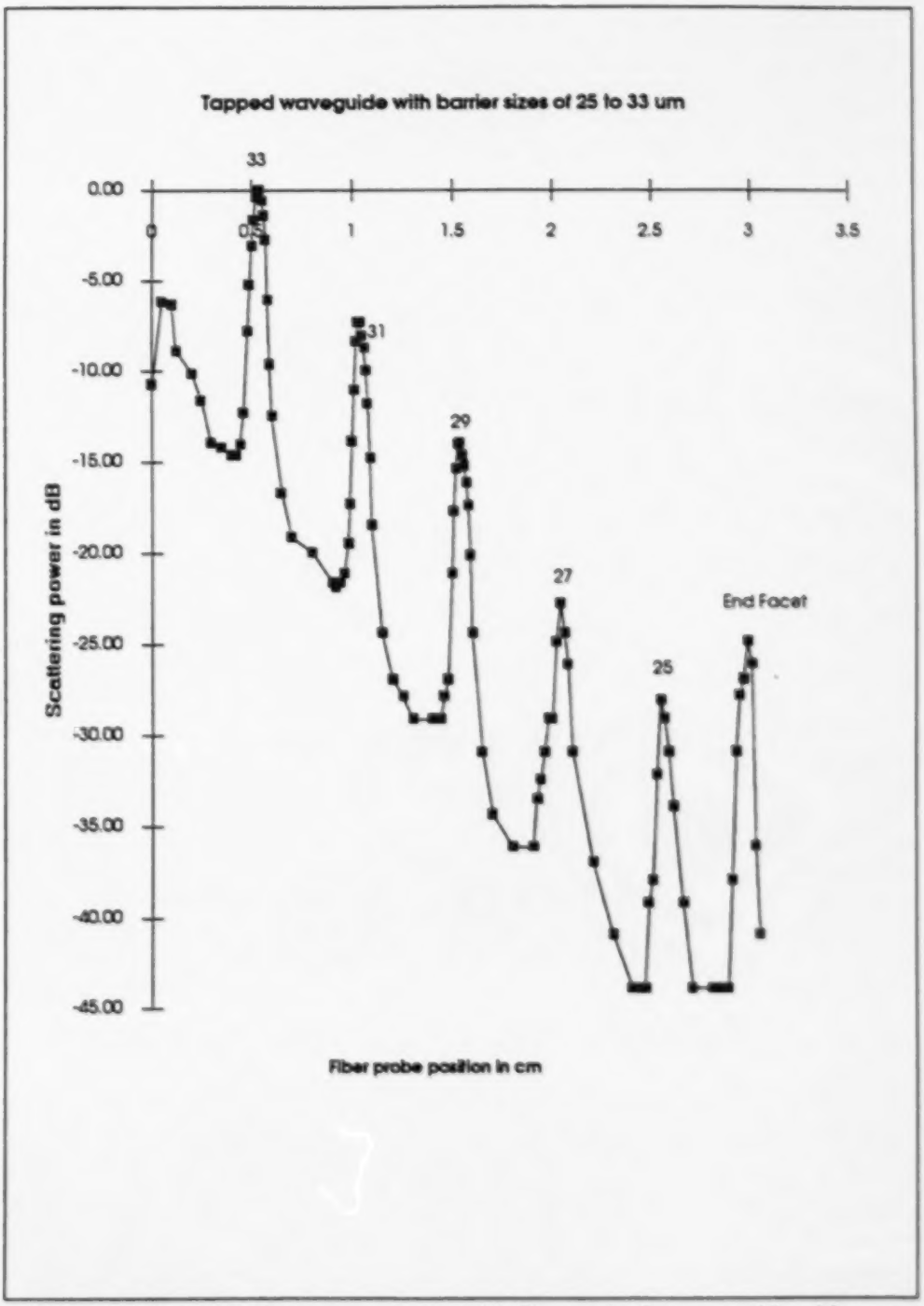


Figure 4.4 Scattering loss measurement with fiber probe for waveguide with taps formed by barrier sizes of 25 to 33 μm

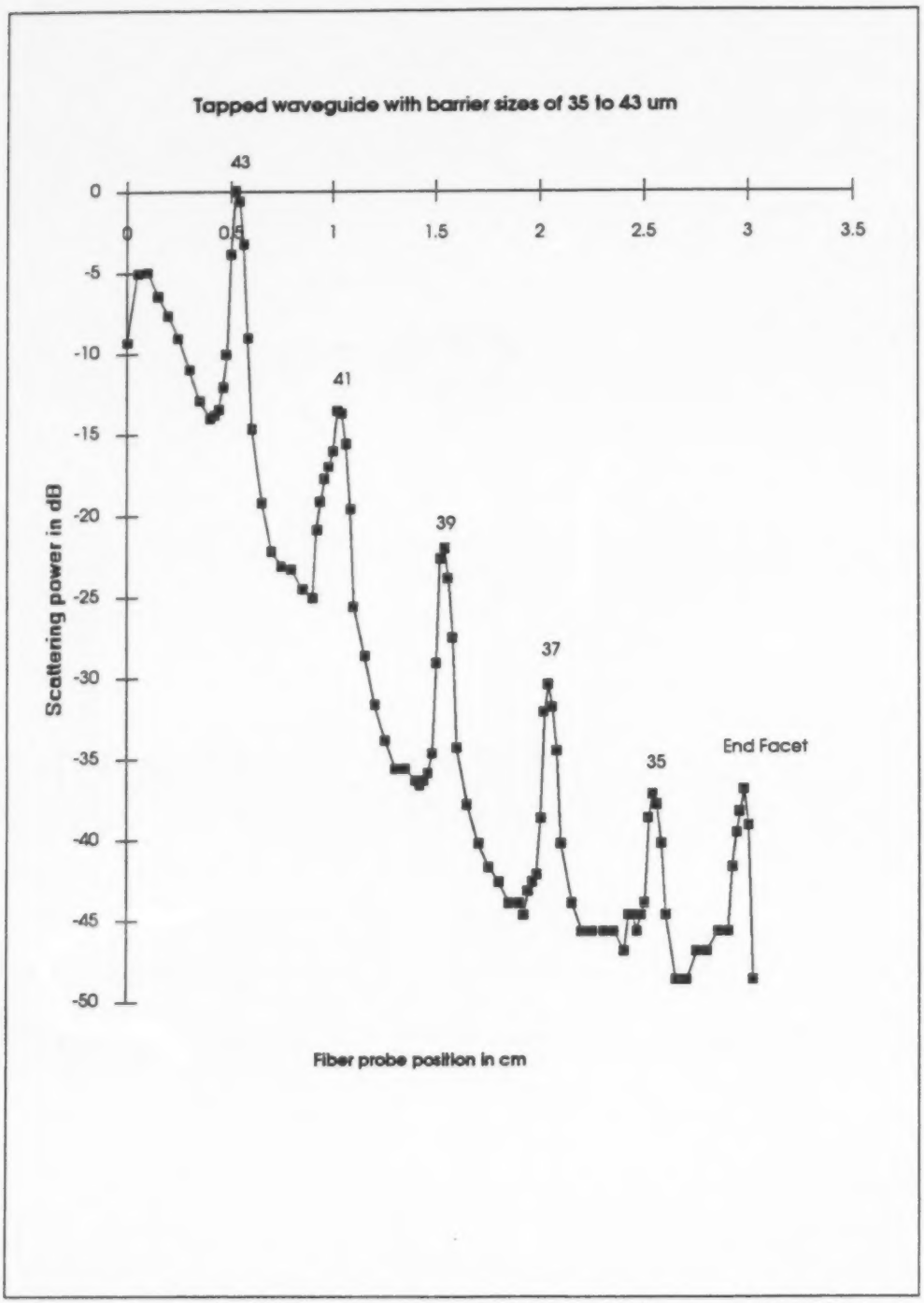


Figure 4.5 Scattering loss measurement with fiber probe for waveguide with taps formed by barrier sizes of 35 to 43 μm

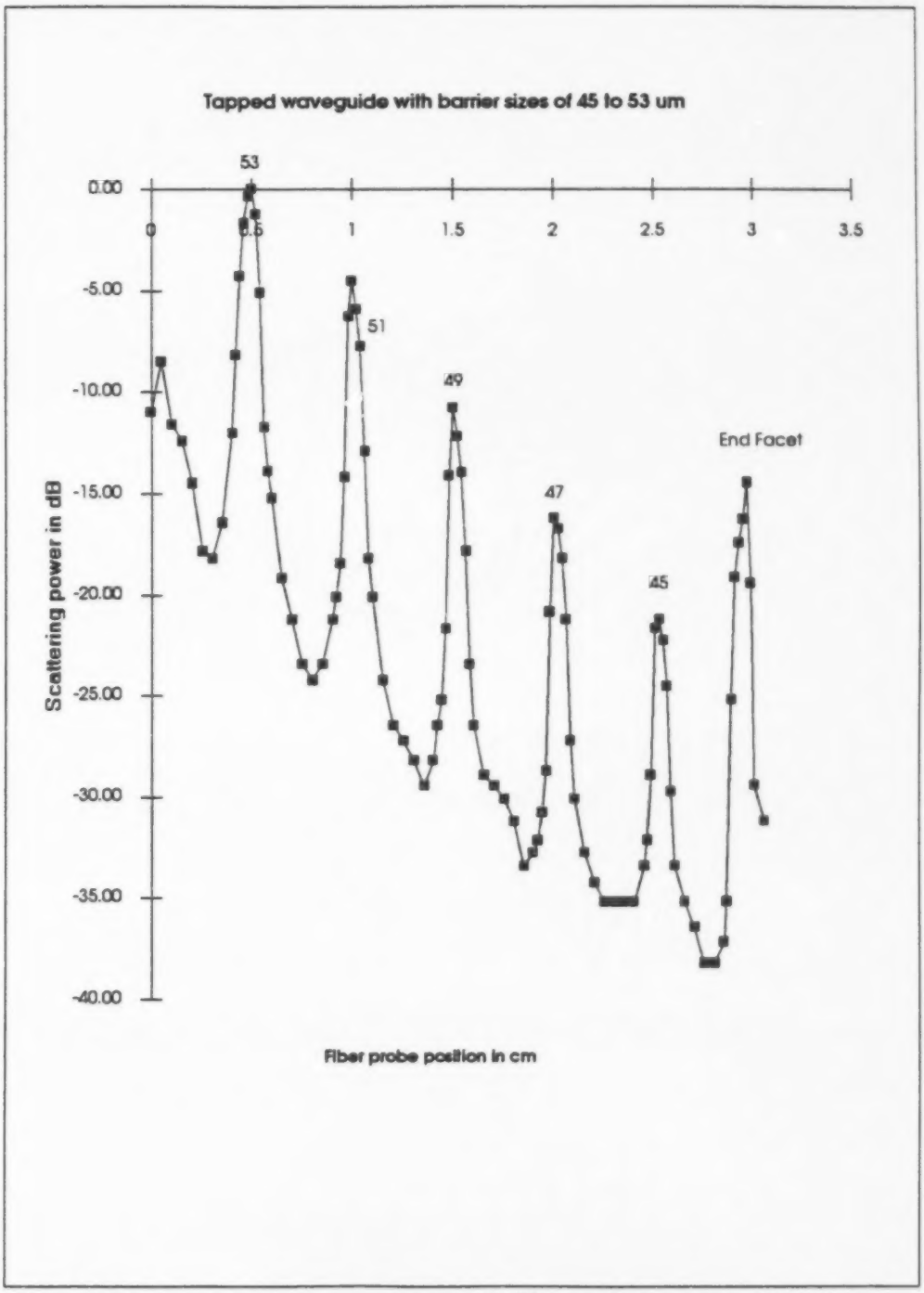


Figure 4.6 Scattering loss measurement with fiber probe for waveguide with taps formed by barrier sizes of 45 to 53 μm

accounted for by the different (111) tapping plane of the end facet, compared to the (112) center taps. The light from the end facet is tapped in a backward direction approximately 30° from the normal of the waveguide surface. The light from the center taps are tapped in a forward direction 30° from the normal of the waveguide surface and will have a different radiation pattern. It was also observed visually that the light in the waveguide is scattered in all directions but at the tapping areas the scattered light is more concentrated at about 30° from the normal of the waveguide. There is also back scattered light at the tapping location of barrier size of 17 μm, which is a poorly formed tap; otherwise, the reflected light from the tapping area is concentrated in the expected directions.

The reflected power from all taps measured both with the fiber probe and with the photodetector are given in Table 4.1.

### 4.4. Analysis of the measured data

Figure 4.7 represents schematically the tapping and attenuation of light in a tapped waveguide. The light coupled into the waveguide reaches the first center tap with power $P_0$. The $i^{th}$ tap has tapping ratio $r_i$ and therefore passes a fraction $(1-r_i)$ of the power. Since the taps in the waveguides are equally spaced, the waveguide attenuation between any two adjacent taps is assumed to be the same with a constant attenuation factor A. $A=10^{-\frac{\alpha L}{10}}$ where $\alpha$ is the constant waveguide transmission loss in dB/cm and L is the separation between taps in centimeters. The last ($N^{th}$) tap is the end facet for which r=1. The following equations then represent the tapped powers along the waveguide:

| Waveguides | 13 to 5 um | | 23 to 15 um | | 33 to 25 um | | 43 to 35 um | | 53 to 45 um | |
|---|---|---|---|---|---|---|---|---|---|---|
| | Fiber | Detector | Fiber | Detector | Fiber | Detector | Fiber | Detector | Fiber | Detector |
| P1 (dB) at $x_1 = 0.0$ cm | 0.00 | 0.00 | 0.00 | 0.00 | 0.00 | 0.00 | 0.00 | 0.00 | 0.00 | 0.00 |
| P2 (dB) at $x_2 = 0.5$ cm | -8.56 | -5.72 | -7.75 | -5.48 | -7.00 | -8.04 | -14.00 | -12.12 | -4.48 | -6.04 |
| P3 (dB) at $x_3 = 1.5$ cm | -9.03 | -10.99 | -9.59 | -10.30 | -14.00 | -14.90 | -22.00 | -21.04 | -10.80 | -13.55 |
| P4 (dB) at $x_4 = 2.0$ cm | -14.89 | -17.52 | -8.61 | -14.82 | -23.00 | -22.30 | -30.00 | -28.61 | -16.10 | -19.09 |
| P5 (dB) at $x_5 = 2.5$ cm | -17.72 | -21.74 | -18.40 | -20.35 | -28.00 | -27.78 | -37.50 | -34.14 | -21.20 | -23.78 |
| P6 (dB) at $x_6 = 3.0$ cm | -12.11 | -18.15 | -10.00 | -8.80 | -25.00 | -28.38 | -37.00 | -36.27 | -14.50 | -25.20 |

Table 4.1 Scattering loss measurement results from both fiber probe and photodetector

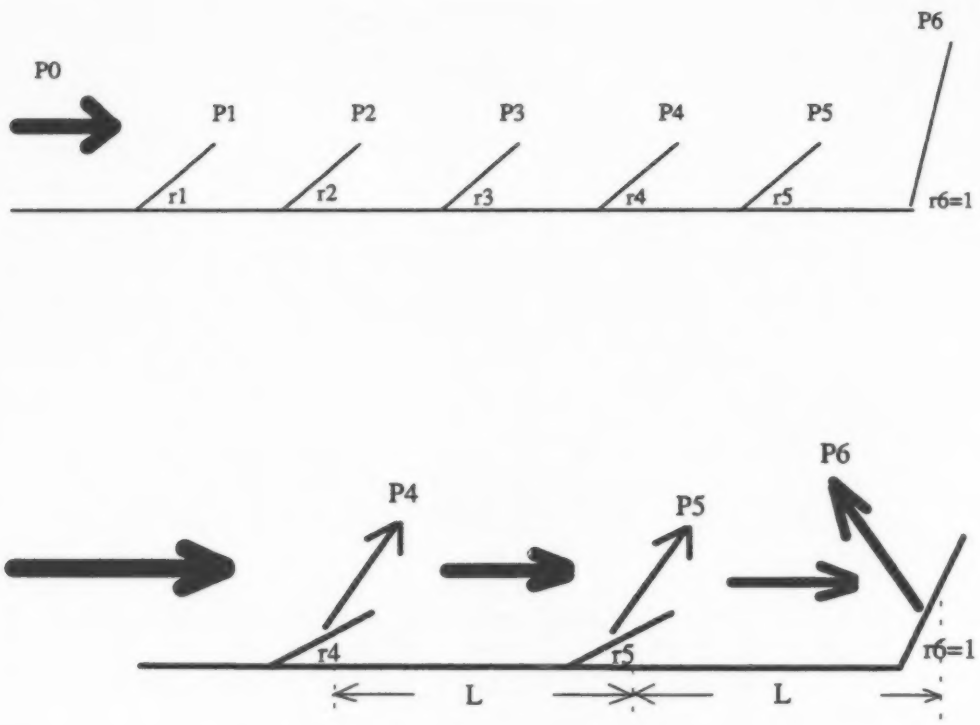


Figure 4.7 Tapping and attenuation in a waveguide

$$P_1 = P_0 r_1$$
$$P_2 = P_0 (1 - r_1) r_2 A$$
$$P_3 = P_0 (1 - r_1) (1 - r_2) r_3 A^2$$
$$P_4 = P_0 (1 - r_1) (1 - r_2) (1 - r_3) r_4 A^3$$
$$P_5 = P_0 (1 - r_1) (1 - r_2) (1 - r_3) (1 - r_4) r_5 A^4$$
...
$$P_i = P_0 (1 - r_1) (1 - r_2) \ldots (1 - r_{i-1}) r_i A^{i-1}$$
...
$$P_N = P_0 (1 - r_1) (1 - r_2) \ldots (1 - r_{N-1}) A^{N-1}.$$

In the experiments, each waveguide consisted of five center taps and an end facet (N=6) and L was equal to 0.5 cm. There are only six equations with seven unknowns. Therefore, an assumption is needed for the analysis to proceed. Various ways of analyzing the measured data have been attempted as described below. The analyzed tapping ratios and transmission losses of all five tapped waveguides measured with both the fiber probe and the photodetector are listed in Tables 4.2 and 4.3 for comparison. Table 4.2 summarizes the analysis of methods A and B and the theoretical tapping ratios. Table 4.3 lists the derived values from method C.

(A) Assume all taps in a waveguide have the same tapping ratio

Since the size difference of our fabricated taps in a single waveguide is small, we assume the tapping ratio difference between center taps in a waveguide is negligible. Then the tapping ratio and transmission loss may be calculated by the relative power radiated from the last two taps and the end facet. The tapped power equations with $r_i = r$ (where i = 1, 2, 3,..., N-1) reduce to [10]:

$$r = \frac{P_5^2}{P_4 P_6} \qquad (4.1)$$

| Waveguides | 13 to 5 um | | 23 to 15 um | | 33 to 25 um | | 43 to 35 um | | 53 to 45 um | |
|---|---|---|---|---|---|---|---|---|---|---|
| Theoretical r | 0.25 | | 0.29 | | 0.33 | | 0.37 | | 0.42 | |
| | Fiber | Photo-detector | Fiber | Photo-detector | Fiber | Photo-detector | Fiber | Photo-detector | Fiber | Photo-detector |
| Method A | | | | | | | | | | |
| r | 0.13 | 0.17 | 0.02 | 0.02 | 0.16 | 0.33 | 0.16 | 0.46 | 0.06 | 0.47 |
| α (dB/cm) | 4.83 | 6.87 | 19.86 | 10.88 | 8.50 | 7.53 | 13.50 | 5.75 | 9.43 | 3.86 |
| Method B | | | | | | | | | | |
| at 7 dB/cm | | | | | | | | | | |
| r1 | 0.10 | 0.16 | 0.07 | 0.03 | 0.18 | 0.34 | 0.28 | 0.42 | 0.08 | 0.38 |
| r2 | 0.08 | 0.16 | 0.23 | 0.05 | 0.21 | 0.35 | 0.42 | 0.40 | 0.10 | 0.33 |
| r3 | 0.13 | 0.25 | 0.07 | 0.06 | 0.42 | 0.46 | 0.54 | 0.51 | 0.13 | 0.35 |
| r4 | 0.06 | 0.27 | 0.05 | 0.07 | 0.49 | 0.50 | 0.60 | 0.64 | 0.22 | 0.47 |
| r5 | 0.16 | 0.31 | 0.11 | 0.10 | 0.52 | 0.59 | 0.87 | 0.82 | 0.24 | 0.46 |
| at 5 dB/cm | | | | | | | | | | |
| r1 | 0.12 | 0.20 | 0.08 | 0.04 | 0.22 | 0.39 | 0.33 | 0.48 | 0.10 | 0.44 |
| r2 | 0.12 | 0.23 | 0.32 | 0.07 | 0.28 | 0.44 | 0.51 | 0.49 | 0.15 | 0.42 |
| r3 | 0.21 | 0.36 | 0.12 | 0.10 | 0.56 | 0.58 | 0.65 | 0.61 | 0.21 | 0.46 |
| r4 | 0.12 | 0.41 | 0.10 | 0.15 | 0.61 | 0.61 | 0.70 | 0.73 | 0.38 | 0.59 |
| r5 | 0.32 | 0.46 | 0.24 | 0.23 | 0.63 | 0.69 | 0.91 | 0.87 | 0.40 | 0.57 |

Table 4.2 Theoretical tapping ratios and analyzed results from Method A and B

| Method C | Fiber Measurement | | | Photodetector Measurement | |
|---|---|---|---|---|---|
| 5-13 um | | | 5-13 um | | |
| all | P=-1.69-8.35*x (dB) | | all | P=-0.14-11.06*x (dB) | |
| 4 out of 5 | P=-4.22-6.67*x (dB) | | 4 out of 5 | P=-0.34-10.92*x (dB) | |
| 3 out of 5 | P=-5.54-6.14*x (dB) | | 3 out of 5 | P=-0.54-10.84*x (dB) | |
| 15-23 um | | | 15-23 um | | |
| all | P=-1.34-7.53*x (dB) | | all | P=-0.18-10.00*x (dB) | |
| 4 out of 5 | P=-3.35-6.19*x (dB) | | 4 out of 5 | P=-0.46-9.82*x (dB) | |
| 3 out of 5 | P=-3.35-7.34*x (dB) | | 3 out of 5 | P=-0.46-9.93*x (dB) | |
| 25-33 um | | | 25-33 um | | |
| all | P=-14.40*x (dB) | | all | P=-0.64-13.96*x (dB) | |
| 4 out of 5 | P=-14.40*x (dB) | | 4 out of 5 | P=-1.60-13.32*x (dB) | |
| 3 out of 5 | P=-14.00*x (dB) | | 3 out of 5 | P=-1.60-13.12*x (dB) | |
| 35-43 um | | | 35-43 um | | |
| all | P=-2.50-18.20*x (dB) | | all | P=-2.23-16.95*x (dB) | |
| 4 out of 5 | P=-6.25-15.70*x (dB) | | 4 out of 5 | P=-5.57-14.73*x (dB) | |
| 3 out of 5 | P=-6.58-15.50*x (dB) | | 3 out of 5 | P=-8.28-13.10*x (dB) | |
| 45-53 um | | | 45-53 um | | |
| all | P=0.29-10.81*x (dB) | | all | P=-0.37-12.12*x (dB) | |
| 4 out of 5 | P=0.72-11.09*x (dB) | | 4 out of 5 | P=-0.92-11.75*x (dB) | |

| | | Fiber Measurement | | | | Photodetector Measurement | | |
|---|---|---|---|---|---|---|---|---|
| Waveguide locations | Wave-guide | aeff (dB/cm) | Tap Loss (dB/cm) | Waveguide Loss (dB/cm) | | aeff (dB/cm) | Tap Loss (dB/cm) | Waveguide Loss (dB/cm) |
| Center of wafer | 53-45 um | 11.00 | 4.73 | 6.27 | | 12.00 | 4.73 | 7.27 |
| | 13-5 um | 7.00 | 2.50 | 4.50 | | 11.00 | 2.50 | 8.50 |
| | 23-15 um | 7.00 | 2.97 | 4.03 | | 10.00 | 2.97 | 7.03 |
| | 33-25 um | 14.00 | 3.48 | 10.52 | | 13.50 | 3.48 | 10.02 |
| Edge | 43-35 um | 17.00 | 4.01 | 12.99 | | 15.00 | 4.01 | 10.99 |

Table 4.3 Analyzed data obtained from Method C

$$\alpha = \frac{10}{L} \mathrm{Log}_{10}\left[ \frac{P_4 (1-r)}{P_5} \right] \qquad \text{dB/cm} \tag{4.2}$$

or if the powers are expressed in decibels, then

$$r = 10^{\left[\frac{2P_5(\mathrm{dB}) - P_4(\mathrm{dB}) - P_6(\mathrm{dB})}{10}\right]} \tag{4.3}$$

$$\alpha = \frac{1}{L}\left[ P_4(\mathrm{dB}) - P_5(\mathrm{dB}) + 10\,\mathrm{Log}(1-r) \right] \quad \text{dB/cm} \tag{4.4}$$

This method of analysis only requires the knowledge of the last two taps and the end facet which has both an advantage and a disadvantage. The advantage is that the analysis only depends on the last three taps. As long as these three taps are well fabricated and there is sufficient light power distributed to these taps, the analysis should be simple. However, any malformations of the last two taps will make this method very inaccurate.

(B) Assigning a value for the waveguide transmission loss $\alpha$ and finding the tapping ratios $r_i$

$\alpha$ can be estimated based on Kumar's report [10] or based on the calculated values from Method C. With the waveguide transmission loss $\alpha$ estimated, the attenuation factor A is then known. After manipulating the tapped power equations, we get:

$$r_{i-1} = \frac{r_i A}{r_i A + \frac{P_i}{P_{i-1}}} \tag{4.5}$$

or

$$\frac{1}{r_{i-1}} = 1 + \frac{P_i}{r_i A P_{i-1}} \tag{4.6}$$

This method provides a way of calculating all r values starting with $r_N$=1. However, errors in measured data will propagate along with the calculations, since the values of $r_i$ are calculated recursively. Also, a good estimation on $\alpha$ is important for obtaining values of $r_i$ accurately.

(C) Using least squares fitting for the tapped powers

Again, since taps in a waveguide are of similar tap sizes, we assume the taps in a single waveguide have the same tapping ratio r. The slope of the linear curve fitting for the tapped powers P in dB versus the distance x in cm represents the effective transmission loss due to tapping and waveguide attenuation. From the effective transmission loss $a_{eff}$ and the predicted tapping ratio, the waveguide transmission loss $\alpha$ can be deduced. For linear attenuation, we approximate the tapped power in dB by the equation

$$P_i = P_c - a_{eff}\, x_i \tag{4.7}$$

where $x_i = 0$ at $i = 1$, and $P_C$ and $a_{eff}$ are determined by the least squares fitting. The measured loss in dB/cm is found to be

$$a_{eff} = \frac{< x_i > < P_i > - < x_i P_i >}{< x_i^2 > - < x_i >^2} \tag{4.8}$$

and

$$P_c = < P_i > + a_{eff} < x_i >. \tag{4.9}$$

The symbol < > indicates average value and $x_i$ and $P_i$ are the $i^{th}$ tap position and power respectively. Since the effective transmission loss is the combination of the losses from the waveguide and from the taps, we have

$$10^{-\frac{a_{eff} L}{10}} = (1-r)10^{-\frac{\alpha L}{10}} \tag{4.10}$$

or

$$\alpha = a_{eff} + \frac{10}{L} \mathrm{Log}_{10}(1-r) \text{ dB/cm} \tag{4.11}$$

The waveguide loss can be obtained by substituting the theoretical tapping ratio in the above equation. Conversely, the average tapping ratio can be found by assuming $\alpha$.

Using this analysis method, the effective transmission loss, which is the slope of the tapped powers, can be obtained. More data are used in this method than the others. (With all five tapped power used to do the curve fitting, Table 4.3 indicates "all".) Also, the line can be modified by eliminating data from poorly fabricated taps. For example, the first tapped power may not be a good datum to take into account because the first tap is close to the input of the waveguide where there may still be uncoupled light in the core. (Table 4.3 indicates as "4 out of 5"; without considering the first tap and the anomalous tap, Table 4.3 indicates as "3 out of 5".) A problem with this approach is that if there is any poorly fabricated tap along a waveguide, the tapped powers obtained after that poor tap may not be correct to use for analysis. The distributed power in the waveguide is disturbed by the poor tap and the assumption for all taps with the same tapping ratio along the waveguide is invalid.

### 4.5. Comparison of the analyzed data

The tapping ratio obtained by the geometric cross-sectional area ratio of the fabricated tap to the waveguide is referred as the theoretical tapping ratio. The theoretical tapping ratios were calculated from tap dimensions measured from the SEM photos. A correction factor of 1.41 was applied to the tapping ratio to account for the polymer depression in the v-groove. Details on the calculations of the correction factor and theoretical tapping ratio are given in Appendix B. The theoretical waveguide transmission loss used is approximately 4 dB/cm with the aluminized waveguide [17]. Tables 4.2 and 4.3 list all the theoretical and the analyzed tapping ratios and transmission losses for comparison.

From Tables 4.2 and 4.3, in general, the analyzed results in method (A) from the measurements with the photodetector agree better with the predicted results than the results from the measurements with the fiber probe. From method (B), the tapping ratios from the photodetector seem more reasonable than from the fiber. The results indicate that the numerical aperture of the fiber may have an effect on the measured data. From method (C), the waveguide transmission loss obtained from photodetector measurement is larger than from fiber measurement.

Since launching conditions and waveguide quality vary from waveguide to waveguide, the comparison of the analyzed data will be within the same waveguide. For the waveguide with taps formed from the barriers of 5 to 13 μm, there is an irregularly shaped tap formed from a 9 μm barrier. This is shown as an overshoot in Figure 4.2 with the fiber probe measurement. However, no such discrepancy appears with the photodetector measurement. The tapping ratios from both measurements are not close to the theoretical one. For the waveguide with barrier sizes of 15 to 23 μm, the tapping ratios resulting from all the methods of analysis disagree with the theoretical one. But as can be seen in the tap photographs, the waveguide tap from the 17 μm barrier has an unexpected tapping surface which contributes to the discrepancies between the measured and theoretical values.

The derived waveguide transmission loss values vary among the analyzing methods. It seems to depend both on the waveguide quality (surface roughness) and on the analyzing methods. The photodetector-measured value of the waveguide with barrier sizes 25 to 33 μm has the closest tapping ratio to the theoretical one in method A. The taps in this waveguide are not too bad. However, it is located second to the edge of the wafer; hence, the loss is higher as calculated from method C. The waveguide with barrier sizes 35 μm to 43 μm has the highest waveguide loss (obtained from method C) among the five waveguides. There is no significant surface

irregularity on the tapping planes shown in the tap photographs. One possibility that may contribute to the inconsistency is that this waveguide is located on the edge of the sample; therefore, as the excess of the polymer was abraded away, some damage had been done to the waveguide. The analyzed values from the photodetector data from the waveguide with barrier sizes 45 to 53 μm are fairly close to the theoretical ones .

From Tables 4.2 and 4.3, inconsistencies in the analyzed data are noticed among different analyzing methods, waveguides, and measurement procedures. Uncertainties in fabrication, measurement and analyzing methods may be the reasons for these inconsistencies as discussed in detail next.

a. The qualities of the tapped waveguides which depend heavily on the fabrication directly affect the scattering loss measurements used here to determine the optical properties of the tapped waveguides. The fabricated taps have anomalous tapping planes other than the expected (112) plane. The unexpected planes may change the tapping ability which affects the assumptions used in analyzing the data. Moreover, the rest of the measured power obtained after the anomalous tap are affected; those data may not be valid for analysis. Such is the case of the irregular center tap from the barrier of 17 μm, where almost all the analyzed values of the tapping ratio for this waveguide are a lot lower than the predicted value. The other source which may influence the qualities of the tapped waveguides is the abrasion process used to make these waveguides. The qualities of the fabricated waveguides seem to relate to the location of the waveguides on the wafer. The surfaces of the waveguides located near the edge of the wafer tend to be scratched more easily than the waveguides located at the center. As a result, the losses of the waveguides near the edge are expected to be higher. Method C applied to measurements both with the fiber and with the photodetector indicate that the waveguides losses near the edge of the wafer are higher than those close to the center. Also, the transmission loss may

vary within the waveguide due to the fabrication quality along the waveguide, which affects the assumption of constant transmission loss along the waveguide used in analyzing the data.

b. Another possible source for peculiar tapping is that air pockets may trapped between the polymer and the tapping surfaces during the application of the polymer. The air pockets may alter the tapping mechanism and the tapped power.

c. Measurement uncertainties, such as different coupling and launching conditions, may prevent the measured data being compared between waveguides.

d. The assumption used in analyzing methods may not represent the actual experimental situations. Modal effects, which have not been considered, may complicate the analysis. Any lack of uniformity of light traveling in the waveguide would make the assumptions invalid. For example, light not filling the entire waveguide may be unable to meet the tapping plane and the reflected power would be reduced. Also the assumption that the scattered light is proportional to the light in the waveguide is not correct. The scattered light is proportional to the amount of light affected by the defects in the waveguide which may not be uniformly distributed.

With these uncertainties, comparison between waveguides and comparison between analyzed data from different methods will not give much insight about the optical properties of the fabricated taps.

# Chapter 5. Conclusions

## 5.1. Summary of work

The most important result of this project is that a new kind of out-of-plane tap for polymer v-groove waveguides in silicon has been developed. Different fabrication procedures were investigated and a satisfactory method was found. The fabrication results in a tap being formed by two intersecting (112) planes at the bottom of the v-groove. Near-vertical tapping has been demonstrated. The radiated power is concentrated at 30° from the normal of the waveguide surface along the light transmitting direction which may be suitable for light distribution in hybrid optoelectronic integrated circuits. The etching mechanism and rates have also been investigated and a linear relationship between the etched distance and the initial barrier size was found. There appear to be different etch rates for different stages of the etching mechanism. However, a model based on constant etch rates which is consistent with these linear relationships is only partially satisfactory. With the information obtained on the etching mechanism and etching rates, a procedure for designing out-of-plane taps of arbitrary size was proposed. Design curves for etching times of 8 and 12 minutes have been obtained. Both the etch time and/or the barrier size can be used to control the tap size formation although the etch time has a more dominant effect on the tap size for the range of barrier sizes tested.

Waveguides with different tap sizes have been fabricated and tested. The optical properties of the tapped waveguides were analyzed in various ways using the data obtained by scattering loss measurements. The tapping performance is directly related to the quality of the tapping surface. We attempted to measure two important

parameters, the tapping ratio and attenuation in a fabricated waveguide. However, the measurement results and the predicted values of the tapping ratios and attenuations are inconclusive. Therefore, the relationship between the designed and fabricated waveguide taps could not be verified.

### 5.2. Suggestions for future work

It is probable that the end facet of the waveguide can be modified, by the same fabrication procedure of the center tap so that it will have the same reflecting surface as the center tap. Then all the radiated light from the serial taps in the waveguide would have the same radiating angle. This possibility is worthy of investigation.

More study of the etching mechanism for center taps is required. A new mask with barriers greater than 50 μm may help in better understanding the etching mechanism and etch rate and provide taps with larger tapping ratios. Also, shorter etch times with less than 4 minutes will provide information on the initial etch rate and mechanism of the center taps. Shorter etch time interval (approximately 1 minute) between etch times of 8 and 12 minutes with different barrier sizes over the full range of the tapping would provide more design curves for various tapping along a waveguide. The EDP etching should be investigated for better homogeneous etching conditions and elimination of the undesirable planes. The application of a cladding layer may help in reducing waveguide loss.

The fabrication of waveguide with taps might be improved with an automated process, especially in the dispensing of the polymer into the v-groove. If the dispensing process is done precisely, the abrasion process for removal of excessive polymer outside of the waveguide can be avoided. As a result, the fabricated waveguides with taps will have higher yield and better and more consistent quality.

The losses can be measured with less uncertainty and the power in an optoelectronic system could be budgeted more accurately.

Moreover, a better measurement setup for evaluating tap performance would help in better understand the tap performance in waveguide. Automation in the measurement would save time, provide consistent measurement conditions for measurement and thus provide more reliable results with less measurement uncertainty or human error. Tap performance at various wavelengths and under different environmental influences should be studied to characterize the waveguide with center taps thoroughly.

## Bibliography


1. L. D. Hutcheson, P. Haugen, and A. Husain, "Optical interconnects replace hardwire," IEEE Spectrum, p. 30, March 1987.

2. S. E. Miller, "Integrated Optics: an introduction," Bell Syst. Tech. J., vol. 48, No. 7, p. 2059, 1969.

3. C. H. Henry, G. E. Blonder, and R. F. Kazarinov, "Glass Waveguides on Silicon for Hybrid Optical Packaging," Journal of Lightwave Technology, vol. 7, p. 1530, 1989.

4. H. Nishihara, M. Haruna, and T. Suhara, Optical Integrated Circuits, McGraw Hill Optical and Electro-optical Engineering Series, 1989.

5. M. Maeda, and H. Nakano, "Integrated Optoelectronics for Optical Transmission Systems," IEEE Communications Magazine, vol. 26, No. 5, p. 45, May 1988.

6. M. Veilleux, A Broadband 10 x 10 Optoelectronic Switch Matrix, Master of Science Thesis, University of Alberta, 1990.

7. T. Miyashita, S. Sumida, and S. Sakaguchi, "Integrated optical devices based on silica waveguide technologies," SPIE vol. 993, Integrated Optical Circuit Engineering VI, p. 288, 1988.

8. Y. Yamada, T. Miya, M. Kobayashi, S. Sumida, and T. Miyashita, "Optical interconnections using silica-based waveguide on Si substrate," SPIE vol. 991, Fiber Optic Datacom and Computer Networks, p. 4, 1988.

9. W. T. Tsang, C. C. Tseng, and S. Wang, "Optical waveguides fabricated by preferential etching," Applied Optics, vol. 14, p. 1200, 1975.

10. S. Kumar, Polymer Waveguides with Taps in Silicon V-grooves, Master of Science Thesis, University of Alberta, 1992.

11. Y. Kokobun, T. Baba, and K. Iga, "Silicon optical printed circuit board for three-dimensional integrated optics," Electronic Letters, vol. 21, p. 508, 1985.

12. M. Abu-Zeid, "Corner Undercutting in Anisotropically Etched Isolation Contours," J. Electrochem. Soc. Solid-State Science and Technology, p.2138, Sep. 1984.

13. G. Fitzpatrick, Alberta Microelectronic Center, private communication.

14. J. E. Goell, and R. D. Standley, "Sputtered glass waveguide for integrated optical circuits," Bell Syst. Tech. J., vol. 48, No. 10, p. 3445, Dec. 1969.

15. N. Nourshargh, E. M. Starr, N. I. Fox, and S. G. Jones, "Simple technique for measuring attenuation of integrated optical waveguides," Electronics Letters, vol. 21, p. 818, 1985.

16. Y. Okamura, S. Yoshinaka, and S. Yamamoto, "Measuring mode propagation losses of integrated optical waveguides: A simple method," Applied Optics, vol. 22, No. 23, p. 3892, Dec. 1983.

17. S. Kumar, private communication.

# APPENDIX A THE PROCEDURE OF HOME MADE ALIGNMENT MARKS

Selective exposure of the photoresist is obtained without a mask. The circular spot from the objective of an optical microscope is used to define the exposed region and the exposure is obtained by removing a UV filter in the light path. A large magnification objective lens gives a small spot size at a shorter exposure time. For example, the exposure time for a 100x objective lens is approximately 5 minutes. After patterning several spots in a column, the wafer is developed and hardbaked. The spots are transferred onto the oxide by dipping the patterned wafer portion into BOE 10:1 solution for 10 minutes and then rinsing in the water cascade. After stripping off the photoresist by acetone and rinsing the wafer by deionized water, the wafer is put into the EDP solution at 115°C for 15 minutes' anisotropic etch. The etchant will etch along the silicon crystal plane and define the right primary flat. The wafer is then rinsed in water cascade and piranha cleaned. A new layer of the photoresist is then spun on the wafer for the center tap waveguide patterns.

# APPENDIX B CALCULATION FOR THEORETICAL TAPPING RATIO AND CORRECTION FACTOR FOR POLYMER DEPRESSION

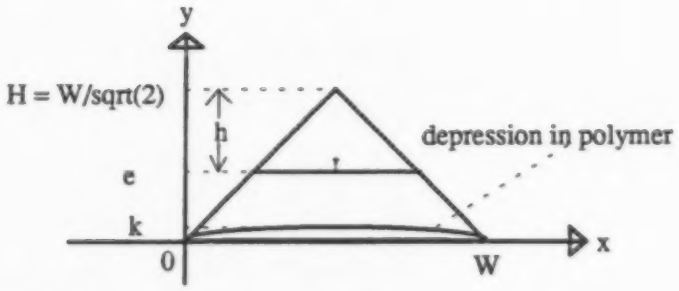


Figure b The end view of the polymer filled v-groove channel waveguide with center tap

Doctorblading of the excessive polymer on the waveguide surface results in depression of the polymer in the v-groove. Therefore, a correction factor should be used to compensate the depression when the theoretical tapping ratio is calculated. A parabolic approximation for the shape of the depression in the polymer should be reasonable.

The equation of a parabola in the geometry of Figure b is

$$y = k - \frac{4k}{W^2}(x - \frac{W}{2})^2$$

The area of the parabola $= \int_0^W y\,dx = \frac{2}{3}kW$

The cross-sectional area of the v-groove $= \frac{1}{2}W\frac{W}{\sqrt{2}}$

The cross-sectional area of the tapping surface $= \frac{t^2}{2\sqrt{2}}$

The theoretical tapping ratio is

$$r = \frac{\text{cross - sectional area of the tapping surface}}{\text{cross - sectional area of the core material in the v - groove}}$$

$$= \frac{\frac{t^2}{2\sqrt{2}}}{\frac{W^2}{2\sqrt{2}} - \frac{2}{3}kW}$$

$$= \frac{1}{1 - \frac{4\sqrt{2}}{3}\frac{k}{W}} \left(\frac{t}{W}\right)^2$$

For a typical waveguide with k = 20 μm, and W = 130 μm

$$r = 1.41\left(\frac{t}{w}\right)^2 = 1.41\left(\frac{h}{H}\right)^2 = 1.41\left(1 - \frac{e}{H}\right)^2.$$

In summary,

$$r = 1.41\left(\frac{\text{Tap width}}{\text{Waveguide width}}\right)^2 = 1.41\left(\frac{\text{Tap height}}{\text{Waveguide depth}}\right)^2$$

$$= 1.41\left(1 - \frac{\text{Etched distance}}{\text{Waveguide depth}}\right)^2.$$